Sensitivity of seawater oxygen isotopes to climatic and tectonic boundary conditions in an early Paleogene simulation with GISS ModelE-R

Christopher D. Roberts,[1,2] Allegra N. LeGrande,[3] and Aradhna K. Tripati[1,4]

Received 7 July 2010; revised 10 June 2011; accepted 30 June 2011; published 12 October 2011.

[1] An isotope-enabled ocean-atmosphere general circulation model (GISS ModelE-R) is used to estimate the spatial gradients of the oxygen isotopic composition of seawater ($\delta^{18}O_{sw}$, where δ is the deviation from a known reference material in per mil) during the early Paleogene (45–65 Ma). Understanding the response of $\delta^{18}O_{sw}$ to changes in climatic and tectonic boundary conditions is important because records of carbonate $\delta^{18}O$ document changes in hydrology, as well as changes in temperature and global ice-volume. We present results from an early Paleogene configuration of ModelE-R which indicate that spatial gradients of surface ocean $\delta^{18}O_{sw}$ during this period could have been significantly different to those in the modern ocean. The differences inferred from ModelE-R are sufficient to change early Paleogene sea surface temperature estimates derived from primary carbonate $\delta^{18}O$ signatures by more than ±2°C in large areas of the ocean. In the North Atlantic, Indian, and Southern Oceans, the differences in $\delta^{18}O_{sw}$ inferred from our simulation with ModelE-R are in direct contrast with those from another $\delta^{18}O$-tracing model study which used different, but equally plausible, early Paleogene boundary conditions. The large differences in $\delta^{18}O_{sw}$ between preindustrial and early Paleogene simulations, and between models, emphasizes the sensitivity of $\delta^{18}O_{sw}$ to climatic and tectonic boundary conditions. For this reason, absolute estimates of Eocene/Paleocene temperature derived from carbonate $\delta^{18}O$ alone are likely to have larger uncertainties than are usually assumed.

Citation: Roberts, C. D., A. N. LeGrande, and A. K. Tripati (2011), Sensitivity of seawater oxygen isotopes to climatic and tectonic boundary conditions in an early Paleogene simulation with GISS ModelE-R, *Paleoceanography*, *26*, PA4203, doi:10.1029/2010PA002025.

1. Introduction

[2] The early Paleogene (65–45 million years ago; Ma) was the warmest period of the last 65 Ma [*Zachos et al.*, 2001]. This interval is thought to have been associated with high background levels of CO_2 [*Pearson and Palmer*, 2000; *Pagani et al.*, 2005], warm high latitudes [*Greenwood and Wing*, 1995; *Fricke and Wing*, 2004; *Sluijs et al.*, 2006; *Bijl et al.*, 2009; *Hollis et al.*, 2009], and warm surface-and-deep oceans [*Lear et al.*, 2000; *Tripati et al.*, 2003; *Zachos et al.*, 2003]. A long-standing challenge for the paleoclimate community has been to accurately estimate early Paleogene surface temperatures and greenhouse gas concentrations. Proxy records indicate that pole-to-equator temperature gradients during the early Paleogene may have been much lower than they are today [e.g., *Greenwood and Wing*, 1995; *Bijl et al.*, 2009; *Hollis et al.*, 2009]. Evidence from fossil leaf morphologies and the distribution of thermophilic fauna and flora indicate that the northern high latitudes (70–80°N) had above freezing cold-month mean temperatures and mean annual temperatures (MATs) >10°C [e.g., *Markwick*, 1994; *Wolfe*, 1994; *Greenwood and Wing*, 1995; *Markwick*, 1998; *Jahren*, 2007]. Marine based proxies have also suggested that Arctic sea-surface temperatures (SSTs) during the early Paleogene may have been as high as 10–25°C [*Tripati et al.*, 2001; *Brinkhuis et al.*, 2006; *Sluijs et al.*, 2006; *Weller and Stein*, 2008]. In contrast, tropical SSTs are estimated to have been similar to or slightly higher than modern values [e.g., *Pearson et al.*, 2001, *Tripati et al.*, 2003; *Zachos et al.*, 2003; *Tripati and Elderfield*, 2004, 2005; *Pearson et al.*, 2007]. *Zachos et al.* [1994] used early Eocene planktic foraminifera (predominantly from the South Atlantic Ocean, the Indian Ocean, and the Southern Ocean) to estimate a SST difference between the tropics and the high latitudes (60–70°S) of only ~10°C; similar gradients were estimated for other intervals of the early Paleogene. Currently, no climate model has been able to accurately

[1]Department of Earth Sciences, University of Cambridge, Cambridge, UK.
[2]Now at Met Office Hadley Centre, Exeter, EX1 3PB, UK.
[3]NASA Goddard Institute of Space Studies and Center for Climate Systems Research, Columbia University, New York, New York, USA.
[4]Institute of the Environment, and Departments of Earth and Space Sciences and Atmospheric and Oceanic Sciences, University of California, Los Angeles, California, USA.

0883-8305/11/2010PA002025

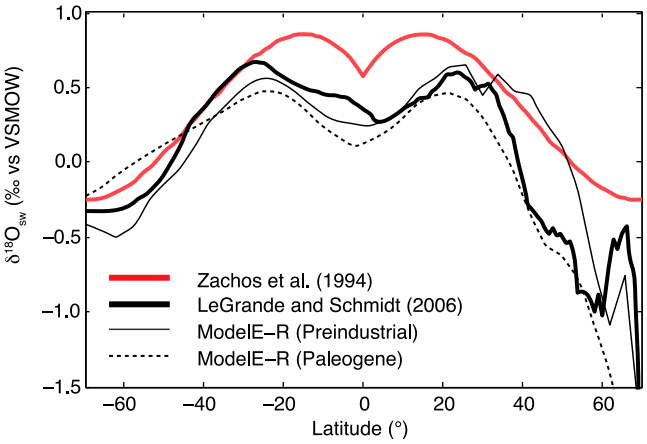

Figure 1. Zonally averaged $\delta^{18}O_{sw}$ from a gridded version of a global $\delta^{18}O_{sw}$ database [*Schmidt*, 1999; *Schmidt et al.*, 1999; *Bigg and Rohling*, 2000; *LeGrande and Schmidt*, 2006] and estimated from the following empirical relationship derived for the southern hemisphere between 0°S and 70°S [*Zachos et al.*, 1994]: $\delta^{18}O_{sw} = 0.576 + 0.41*\lambda + 0.0017*\lambda^2 + 1.35*10^{-5}*\lambda^3$ (where λ is latitude). Zonal averages from preindustrial and Paleogene simulations with GISS ModelE-R are also included for comparison. Paleogene values are adjusted to have a global mean $\delta^{18}O_{sw}$ of zero to allow comparison with modern values.

simulate conditions consistent with all of the proxy data when configured with appropriate boundary conditions, including the high levels of CO_2 estimated by geochemical proxies [e.g., *Huber and Sloan*, 2001; *Tindall et al.*, 2010]. Simulations with increased greenhouse gas concentrations result in higher global mean temperatures (and above-freezing polar conditions), but, in the absence of additional feedback mechanisms, meridional temperature gradients remain much higher than those inferred for the early Paleogene. This means that it is possible to simulate higher polar temperatures, but only at the expense of unrealistically high tropical temperatures.

[3] The $^{18}O/^{16}O$ ratio of fossil carbonate, particularly foraminiferal calcite, is one of the oldest and most widely applied proxies in paleoceanography [e.g., *Emiliani*, 1955; *Shackleton and Opdyke*, 1977; *Zachos et al.*, 2001]. Such measurements are one of several lines of evidence that have been used to infer low latitudinal gradients of sea-surface temperature during the early Paleogene [e.g., *Zachos et al.*, 1994; *Hollis et al.*, 2009]. Throughout this paper, water $\delta^{18}O$ is quoted relative to Vienna standard mean ocean water (VSMOW), and carbonate $\delta^{18}O$ is quoted relative to the Vienna Pee Dee Belemnite (VPDB) carbonate standard. (These two standards are offset by 0.27‰.) The $\delta^{18}O$ of carbonate ($\delta^{18}O_c$) precipitating from seawater is controlled by both temperature and the $\delta^{18}O$ of seawater ($\delta^{18}O_{sw}$). In the absence of other confounding influences—such as species-specific 'vital' effects [*Wefer and Berger*, 1991], a pH/CO_3^{2-} effect on $\delta^{18}O_c$ [*Spero et al.*, 1997; *Zeebe*, 1999, 2001], and dissolution or recrystallization of fossil carbonate [*Pearson et al.*, 2001]—quantitative determination of ocean temperatures from measurements of $\delta^{18}O_c$ also requires the estimation of $\delta^{18}O_{sw}$. On geological timescales, global mean $\delta^{18}O_{sw}$ is controlled by the volume (and isotopic composition) of water and ice stored on the continents and, to a lesser extent, the weathering and deposition of hydrous and/or oxygen bearing sediments and evaporites (e.g., gypsum). Spatial gradients of $\delta^{18}O_{sw}$ are affected by precipitation, evaporation and river runoff (and the isotopic composition of these fluxes), freezing and melting of ice, and ocean mixing and advection [*Craig and Gordon*, 1965]. This means that $\delta^{18}O_{sw}$ essentially acts as a tracer of freshwater, with more negative values correlated with lower salinities. Importantly, all of the variables considered above are impacted by climatic and tectonic boundary conditions meaning that it is likely that $\delta^{18}O_{sw}$ gradients in the geological past were different to those in the modern ocean.

[4] Independent of carbonate $\delta^{18}O$ measurements, there are no proxy-based constraints on spatial gradients of $\delta^{18}O_{sw}$ during the Paleogene, and as a result, modern gradients have been used for paleotemperature estimations. For example, *Zachos et al.* [1994] derived an empirical relationship between latitude and $\delta^{18}O_{sw}$ for the modern oceans. In the absence of other constraints, this relationship (with an appropriate correction to the average $\delta^{18}O_{sw}$ to account for changes in continental ice storage) has been widely used as a reasonable approximation of latitudinal $\delta^{18}O_{sw}$ gradients in the past. Comparison of the *Zachos et al.* [1994] relationship with the zonal mean from a gridded version of a global $\delta^{18}O_{sw}$ [*LeGrande and Schmidt*, 2006] (Figure 1) demonstrates that, although the match in the southern hemisphere is good, the fit in the tropics and northern hemisphere is poor. This mismatch likely results from the fact that the empirical relationship derived by *Zachos et al.* [1994] is only fit to $\delta^{18}O_{sw}$ data from the southern hemisphere. Simple latitude-vs-$\delta^{18}O_{sw}$ relationships are insufficient to describe the meridional $\delta^{18}O$ gradient in the northern hemisphere because of the difference in mean $\delta^{18}O_{sw}$ between the North Pacific and North Atlantic, and the presence of restricted basins and marginal seas such as the Mediterranean Sea and the Arctic Ocean.

[5] Early Paleogene $\delta^{18}O_{sw}$ gradients need to be assessed to improve $\delta^{18}O_c$ estimates of spatial gradients of SST during hothouse periods such as the Paleocene and Eocene. Such studies are also useful for evaluating the response of meridional temperature gradients to changes in the mean climate state. The ocean-atmosphere general circulation model GISS ModelE-R fully incorporates water isotopes into the hydrological cycle, making it a useful tool for estimating $\delta^{18}O_{sw}$ gradients in the geological past. To date, three other models have been used to simulate $\delta^{18}O_{sw}$ during 'greenhouse' intervals [*Roche et al.*, 2006; *Zhou et al.*, 2008; *Tindall et al.*, 2010].

2. Methods

2.1. GISS ModelE-R

[6] We simulate preindustrial (PI) and early Paleogene climates using the National Aeronautics and Space Administration Goddard Institute for Space Studies (NASA GISS) ModelE-R. ModelE-R is a coupled atmosphere-ocean, water isotope-enabled, general circulation model with a horizontal resolution of 4° × 5° (latitude × longitude) in the ocean and atmosphere.

[7] The atmosphere component of ModelE used in this study has 20 vertical layers in the atmosphere, with terrain-

following 'sigma' coordinates up to 150 hPa and pressure coordinates between 150 hPa and 0.1 hPa [*Schmidt et al.*, 2006]. The ocean component of ModelE-R is a mass-conserving model with a free-surface and a vertical resolution of up to 13 layers in mass/pressure coordinates [*Russell et al.*, 1995, 2000; *Liu et al.*, 2003]. Ocean interior and boundary layer vertical mixing is performed using the k-profile parameterization (KPP) of *Large et al.* [1994]. The impacts of isopycnal diffusion and mesoscale eddy-induced tracer transports are parameterized as by *Gent and McWilliams* [1990] and *Gent et al.* [1995] using the variable transfer coeffcients of *Visbeck et al.* [1997] and the skew-diffusive formulation of eddy-transport velocity of *Griffies* [1998]. Horizontal tracer advection in the ocean is performed using a quadratic upstream scheme. This scheme treats both the mean and directional gradients within grid-boxes as prognostic variables allowing sharp (grid-box scale) gradients in tracer concentration to be preserved during advection. Sea-ice in ModelE-R has the same horizontal resolution as the ocean and atmosphere, four thermodynamic layers, and is allowed to advect ice with a viscous-plastic rheology [*Zhang and Rothrock*, 2000; *Liu et al.*, 2003; *Schmidt et al.*, 2004].

[8] Water tracers (H_2O, HDO and $H_2^{18}O$) in ModelE-R are conservatively traced throughout the ocean, atmosphere and land-surface [*Aleinov and Schmidt*, 2006; *Schmidt et al.*, 2007]. All freshwater fluxes (precipitation, evaporation, runoff, sea-ice formation and melting) have an isotopic composition and are associated with appropriate isotopic fractionations at phase changes. Water isotopes in the land surface scheme are only fractionated during evaporation from bare soil and the canopy. There is no fractionation during phase changes in the soil, during runoff or during transpiration [*Aleinov and Schmidt*, 2006]. ModelE-R captures the major features of $\delta^{18}O_{sw}$ present in the modern ocean and has a strong correlation between modeled and observed $\delta^{18}O_{sw}$ fields (area weighted $r^2 = 0.77$) [*LeGrande and Schmidt*, 2006; *Schmidt et al.*, 2007].

2.2. Early Paleogene Configuration of ModelE-R

[9] Paleogeographic boundary conditions were derived from the 2° × 2° gridded topography and bathymetry data set used by *Bice and Marotzke* [2002]. The land-sea distribution and continental topography are based on an early Eocene reconstruction [*Scotese et al.*, 1998; *Bice et al.*, 2000] and the bathymetry was originally reconstructed by *Bice et al.* [1998] using a seafloor age-depth relationship. The 2° × 2° data were re-gridded to create a land-sea mask and topographic data at the 4° × 5° resolution required by ModelE-R. The maximum depths of several shallow seaways (the Tasman Seaway, Drake Passage, Greenland-Norway seaway and Turgai Strait) were explicitly specified to be ~249 m deep. River runoff was directed to follow the steepest topographical gradients, with some adjustments to prevent the accumulation of water in closed drainage basins.

[10] Vegetation boundary conditions were derived from a gridded Eocene vegetation reconstruction [*Sewall et al.*, 2000], which was based on Paleogene floral reconstructions [*Wing*, 1998a, 1998b; *Rull*, 1999; *Wilf*, 2000]. This reconstruction was translated to the 4° × 5° ModelE-R land-mask and the vegetation types were described as proportions of the plant functional types used by ModelE-R (bare soil, tundra, grassland, grassland with shrub cover, grassland with tree cover, deciduous forest, evergreen forest, rain forest). The resulting distribution of vegetation determined land-surface characteristics (roughness length, snow masking depth, field capacity and seasonally varying albedo) as described by *Matthews* [1984]. Lakes were initialized with a uniform surface fraction (5%) and depth (10 m).

[11] Atmospheric concentrations of CO_2 and CH_4 were set at 4 × preindustrial CO_2 and 7 × preindustrial CH_4 (equivalent to ~4.3 × preindustrial CO_2), estimates that fall within the ranges estimated for the early Paleogene [*Pearson and Palmer*, 2000; *Pagani et al.*, 2005; *Royer*, 2006; *Beerling et al.*, 2009; *Bartdorff et al.*, 2008; *Sloan et al.*, 1999, p. 276]. Orbital parameters (eccentricity = 0.027, obliquity = 23.2°, longitude of perihelion from equinox = 180°) were chosen to be intermediate values from a range of Paleogene values estimated using the calculations of *Laskar et al.* [2004] and solar luminosity was held constant at the modern day value. The impact of these orbital changes was to increase incident solar radiation at the top of the atmosphere by an average of 0.1 W/m^2.

[12] Mean ocean salinity was adjusted to have a salinity of 35.7 parts per thousand (ppt). This value is within the range (35.1–36.2) estimated for the Eocene [*Hay et al.*, 2006] when the volume of water in each component of the hydrosphere and rates of evaporite weathering and deposition are considered. Accurate estimation of the global mean $\delta^{18}O$ of seawater is not relevant for the simulation of $\delta^{18}O$ gradients. In all our comparisons with paleo-observations, we used a value of −0.81 ‰ (estimated assuming ice-free conditions and an average $\delta^{18}O$ composition of −40 ‰ for modern Antarctic ice, −30 ‰ for other continental ice). In the absence of independent constraints, we note that (to an extent) global mean $\delta^{18}O$ is a free variable that could be tuned to give the best agreement with observations.

[13] To reduce long integration times, the Paleogene simulation was initialized using boundary conditions derived from zonally averaged ocean conditions from a 500 year simulation which was forced with 4 × preindustrial CO_2 (but was otherwise identical to the preindustrial control). To further reduce 'spin-up' time, the Paleogene initial conditions at latitudes higher than 60°N/S were set equal to values at ±60° and, in each water column, ocean levels 11–13 were set equal to those at level 10. The Paleogene simulation was then allowed to evolve freely for 2000 years. The initial conditions should not have affected the resulting equilibrium climate. The 4 × preindustrial CO_2 run was initialized from a long preindustrial control simulation [*Schmidt et al.*, 2007], which itself was initialized from the *Levitus et al.* [1994] ocean climatology. All Paleogene climatologies presented in this study are calculated from the last 100 years of the 2000 year simulation. During these 100 years, global mean temperatures were increasing by <0.01°C/century in the surface ocean and ~0.05°C/century in the deepest ocean layer (except in the Arctic, where the temperature of the deepest ocean layer was decreasing by 0.1°C/century).

3. Results

3.1. Summary of Simulated Paleogene Climate

[14] The early Paleogene simulation is characterized by extreme warmth (Figure 2) and an intensified hydrological cycle (Figure 3). Mean annual surface air temperature (SAT)

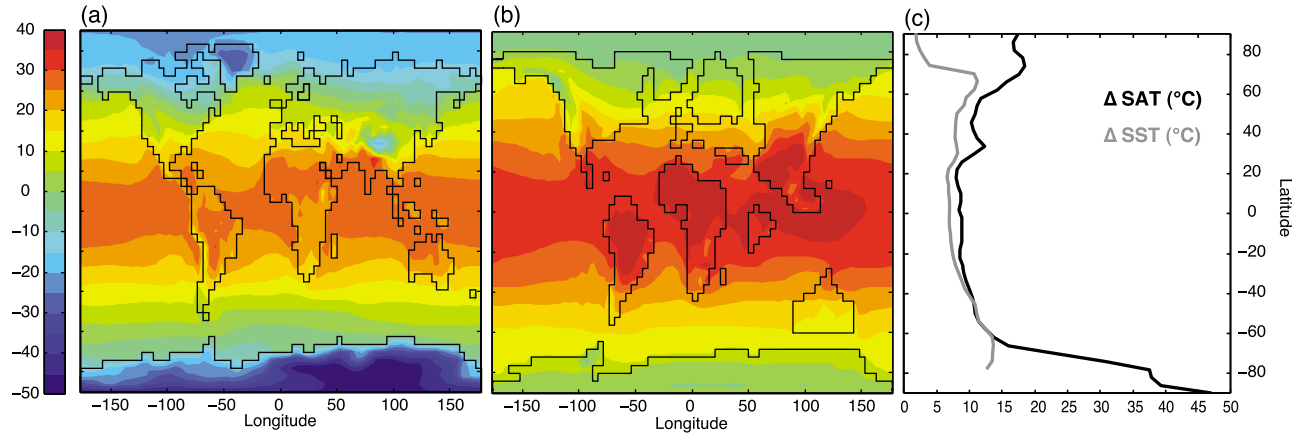

Figure 2. Surface temperatures (°C) in the Paleogene and preindustrial simulations: (a) mean annual surface air temperature (SAT) in the preindustrial control simulation, (b) mean annual SAT in the Paleogene simulation, (c) difference (Paleogene – preindustrial) in zonal mean SAT and SST.

in the Paleogene simulation is 25°C, compared to 14°C in the PI control. Other global climate statistics are summarized in Table 1. Figure 2 shows the considerable amplification of warming at higher latitudes in the Paleogene simulation. About half of the warming over the South Pole is due to the removal of the Antarctic ice sheet and the associated ~2 km reduction in mean elevation (both simulations have an Antarctic lapse rate of ~10°C/km). Annual mean surface air temperatures (SATs) in the Arctic increased from −17°C to −2°C, and Arctic SSTs increased from −2.7°C to −0.7°C.

[15] Continental seasonality is generally increased in the Paleogene simulation with the largest annual range of SATs at 50–60 °N in the interior of the Asian and North American continents. In these regions, winter temperatures are subfreezing and summer temperatures exceed 40°C. The summer temperature extremes are particularly evident in the Asian continent at ~30°N where they reach >55°C during June–July–August (JJA) and are associated with extremely low precipitation (<20 mm/year) and hence an absence of evaporative cooling. Simulated SATs and precipitation imply that this region would have been a desert during the Paleogene, in conflict with fossil vegetation which indicate that this region was covered with deciduous and tropical forest [*Utescher and Mosbrugger*, 2007]. This inconsistency is likely due to uncertainties in the applied model boundary conditions (e.g., topography prescribed in the southeast of the Asian continent).

3.2. Surface Freshwater Balance

[16] Relative to the PI control, the Paleogene simulation shows an intensification of the hydrologic cycle with a large increase in moisture convergence in equatorial regions, an intensification and expansion of the sub-tropical regions of net evaporation, and a small increase of precipitation minus evaporation (P–E) in the high latitudes. These changes are associated with a large increase in river runoff into the oceans at the equator and in the high-latitudes (Figures 3 and 4). The increased transport of atmospheric moisture in the Paleogene midlatitudes is associated with an increase in poleward latent heat transport of ~0.9 Petawatts (PW) at 40°N. Figure 5 shows the $\delta^{18}O$ composition of precipitation ($\delta^{18}O_p$) in both simulations. Less negative high-latitude $\delta^{18}O_p$ in the Paleogene simulation is a consequence of the higher global temperatures, the reduced meridional temperature gradient, and the increased atmospheric transport of heat, moisture and $H_2^{18}O$ in the midlatitudes (Figure 5). However, $\delta^{18}O_p$ over the North Atlantic is lower in the Paleogene simulation, likely indicating a local source effect from the North Atlantic surface ocean (where $\delta^{18}O_{sw}$ is lower in the Paleogene simulation). In both simulations, the isotopic composition of river runoff largely reflects the isotopic composition of precipitation over catchment areas.

3.3. Ocean Climatology and Circulation

[17] Simulated Paleogene ocean warming (relative to the PI control) is most significant in the southern high latitudes and the abyssal ocean where temperatures are 8–12°C higher than those in the PI control (Figure 6). In comparison, thermocline and surface ocean temperatures in the tropical oceans are only 5–7°C higher than those in the PI control.

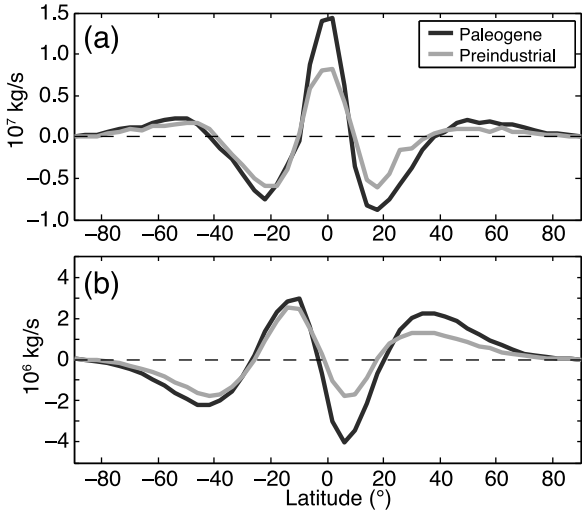

Figure 3. (a) Precipitation minus evaporation (P–E) weighted by area for each latitudinal band, (b) total northward transport of $H_2^{18}O$ in the atmosphere for each latitude.

Table 1. Selected Global Mean Climate Statistics

Climate variable	Preindustrial	Paleogene
Surface air temperature (SAT) (°C)	13.8	24.9
Sea-surface temperature (SST) (°C)	18.0	26.7
Sea-surface salinity (ppt)	35.0	35.7
Precipitation/Evaporation (mm/day)	3.0	3.7
Total cloud cover (%)	59	57
Total atmospheric water vapor (kg/m^2)	23.6	49.3
Planetary albedo (reflected/incident SW @ TOA) (%)	29.5	27.1
Surface albedo (reflected/incident SW @ surf.) (%)	12.3	7.8
Ocean surface albedo (reflected/incident SW @ surf.) (%)	7.1	5.8
Land surface albedo (reflected/incident SW @ surf.) (%)	24.4	12.5

The highest SSTs in the Paleogene simulation exceed 35°C and occur in the equatorial regions to the east and west of Africa and in the west of the Pacific basin. Despite the global warmth of the Paleogene simulation, the lowest ocean temperatures in the Arctic Ocean are associated with seasonally forming sea-ice. However, ModelE-R has a known deficiency in its distribution of sea-ice in simulations of modern climate: compared to observations and other models, there is too much ice in the northern hemisphere and the seasonal cycle is reduced [*Hansen et al.*, 2007; *Stroeve et al.*, 2007]. In addition, of the 15 models used in sea-ice simulations for the 4th IPCC assessment report [*Solomon et al.*, 2007], ModelE-R had the largest Arctic summer sea-ice extent and the smallest reduction in Arctic sea-ice area in response to warming during the next 100 years [*Zhang and Walsh*, 2006].

[18] Compared to the PI control, Paleogene salinities are increased by 1.5 ppt in the upper 1500 m of the Southern Ocean, (recall that mean ocean salinity was increased by 1 ppt). The salinity gradient between the equatorial thermocline and surface ocean is also increased due to more negative P–E in the subtropics and increased P–E at the equator. At low latitudes, the open Panama and Tethys seaways inhibit the development of zonal salinity gradients between ocean basins in the Paleogene simulation. Salinities in the Arctic are much lower due to the combined impact of increased basin isolation and increased freshwater forcing (precipitation − evaporation + runoff; P–E+R), about two thirds of which is due to increased river runoff. The low salinities in the Arctic surface ocean (<20 ppt) result in a very stable vertical density profile.

[19] Unlike the PI control, the Paleogene simulation has no strong circumpolar current in the Southern Ocean (Figure 7). This is likely to be a result of the very shallow Southern Ocean gateways and more southerly position of the Australian continent in the Paleogene configuration, both of which act as barriers to zonal flow and encourage the development of geostrophic gyres. The Paleogene simulation also has stronger subtropical gyres and western boundary currents in the Pacific Ocean, a westward flowing subequatorial current circling the globe through the open Tethys Ocean and Panama seaways, and stronger sub-polar gyres in the Ross Sea and Weddell Sea. Global meridional overturning in the Paleogene simulation (Figure 8) is nearly symmetrical, with less cross-equatorial transport compared to the PI simulation. Deep circulation in the PI control is dominated by a cross-equatorial deep overturning cell in the Atlantic (25 Sv) and excessive overturning at intermediate depths in the North Pacific (23 Sv). In contrast, global overturning in the Paleogene simulation is accommodated by two cells of approximately equal magnitude (30–35 Sv) with maxima at ±60° latitude and ~1500 m depth with deep water formation in the North Pacific and the Southern Ocean. There is no significant overturning in the North Atlantic. However, a further Paleogene simulation (not presented) has shown that North Atlantic overturning in ModelE-R is

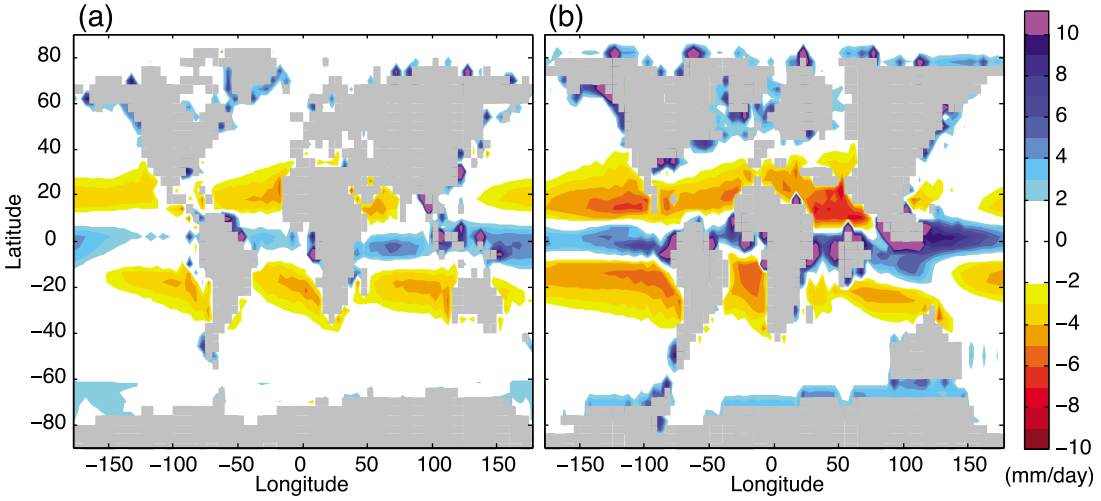

Figure 4. Simulated freshwater forcing (precipitation minus evaporation plus runoff; P–E+R) at the surface ocean in (a) the preindustrial simulation and (b) the Paleogene simulation.

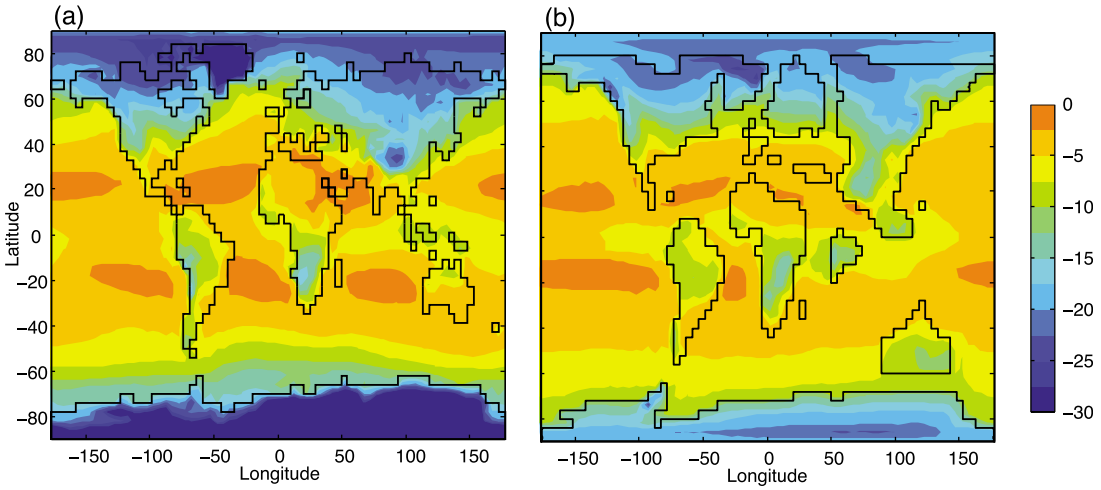

Figure 5. Precipitation δ^{18}O (per mil vs VSMOW) from (a) the preindustrial simulation and (b) the early Paleogene simulation.

sensitive to the degree of oceanic exchange of salt and freshwater between the North Atlantic and Arctic Oceans [*Roberts et al.*, 2009].

3.4. Heat Transport

[20] Figure 9 shows northward heat transport for the Paleogene and PI simulations broken down into the following three components: (1) total heat transport, (2) ocean heat transport, and (3) atmospheric heat transport. Total heat transport is very similar in both simulations and peaks at 5.5 PW at ±36° latitude in the Paleogene simulation compared to 5 PW at ±36° latitude in the PI control. In the ocean, there is 0.5 PW less net heat transport from the southern to the northern hemisphere in the Paleogene simulation (Figure 9c). Despite the significant differences in global climate, maximum total heat transport in both simulations falls within the range of values estimated for the modern climate system (4.1–6.4 PW) [*Wunsch*, 2005]. This result is consistent with work by *Stone* [1978] who showed that total meridional heat transport is relatively insensitive to the details of ocean and atmosphere dynamics and its magnitude is largely constrained by the solar constant, Earth's obliquity, and mean albedo.

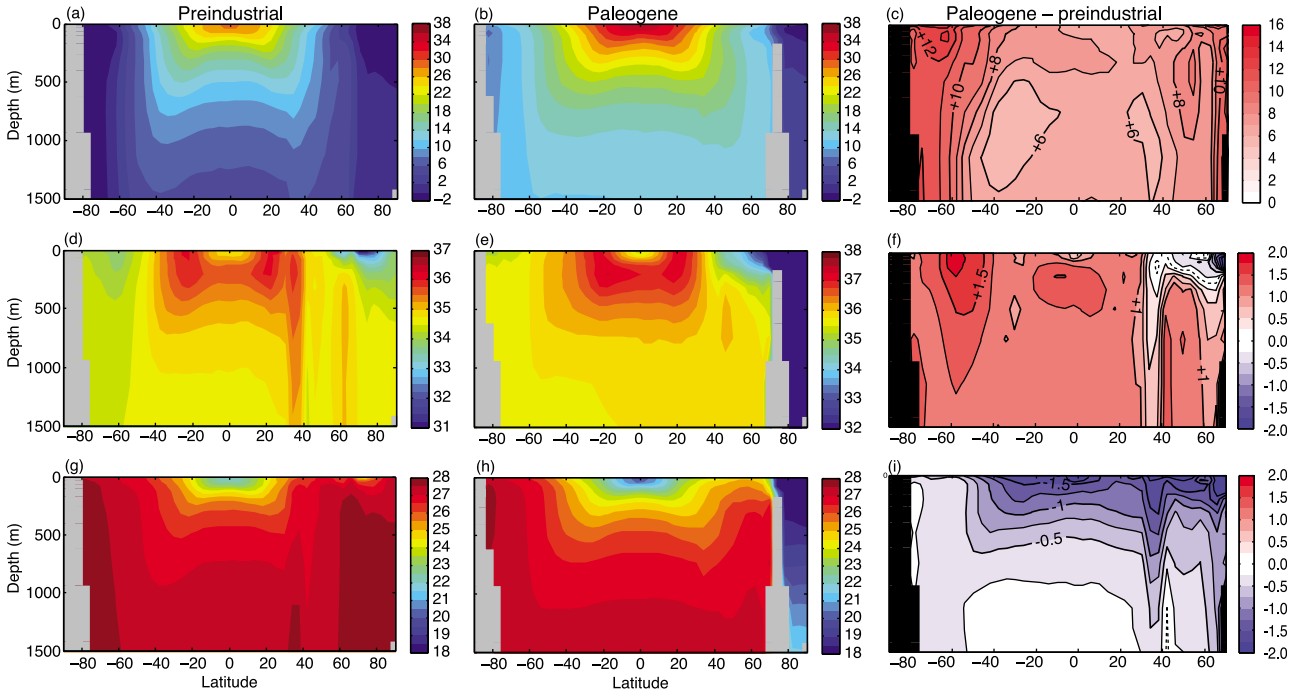

Figure 6. Ocean zonal averages and difference plots from preindustrial and early Paleogene simulations: (a–c) mean annual potential temperature (°C), (d–f) mean annual salinity (ppt), and (g–i) mean annual potential density (kg/m^3).

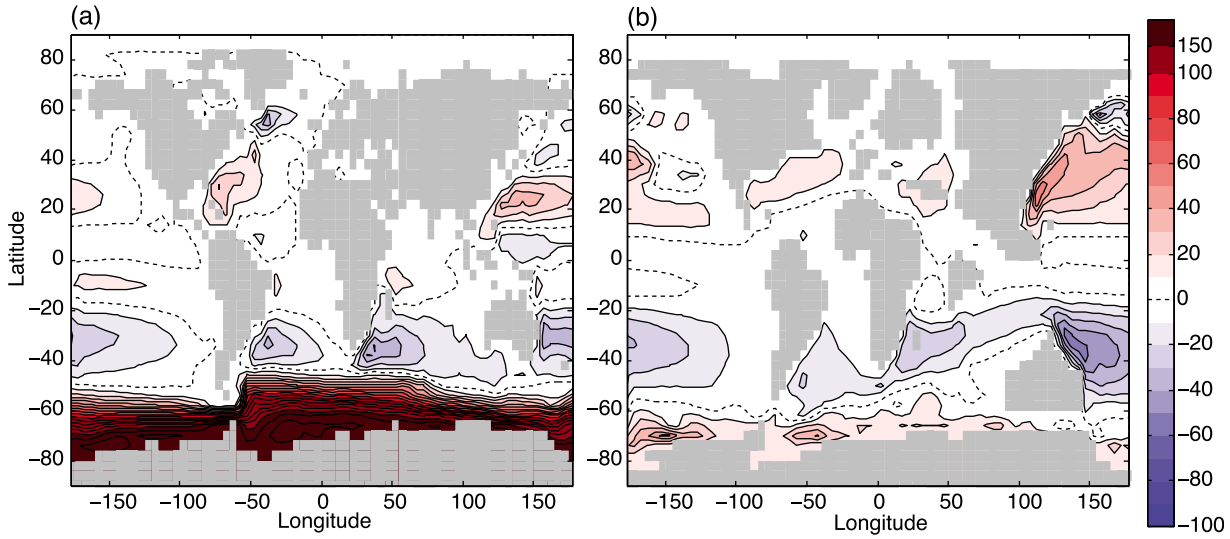

Figure 7. Vertically integrated horizontal transport in the ocean (barotropic stream function) in Sverdrups (Sv) for (a) the preindustrial simulation and (b) the Paleogene simulation.

3.5. Surface Ocean $\delta^{18}O_{sw}$

[21] Maps of surface ocean $\delta^{18}O_{sw}$ from the Paleogene and PI simulations are shown in Figure 10 and zonal averages from both simulations are included in Figure 1. To aid comparison with the PI simulation, Paleogene $\delta^{18}O_{sw}$ values in Figures 1 and 10 are plotted with a global mean $\delta^{18}O_{sw}$ of zero (as noted earlier, this adjustment does not affect the spatial gradients); these adjusted values are used in the comparisons in the text below. The main features of the surface ocean $\delta^{18}O_{sw}$ distributions are shared by both the PI and Paleogene simulations (Figures 1 and 10). They each show local minima around the equator, sub-tropical maxima, and lower values in the high latitudes. The most significant differences in the Paleogene simulation relative to the PI control are (1) much lower salinities and $\delta^{18}O_{sw}$ in the Arctic, North Atlantic, and Tethys/Mediterranean Oceans, (2) higher salinities and $\delta^{18}O_{sw}$ in the Southern Ocean and western equatorial Pacific, and (3) expanded salinity and $\delta^{18}O_{sw}$ minima in the equatorial oceans surrounding the continents.

[22] The reduced $\delta^{18}O_{sw}$ values in the Arctic, North Atlantic and Tethys Oceans in the Paleogene simulation are associated with a more positive surface freshwater forcing (P-E+R), a more restricted Arctic basin configuration, and a reduced ocean transport of salt and $H_2^{18}O$ from the sub-tropics due to the absence of a meridional overturning circulation and a weaker sub-tropical gyre in the North Atlantic. An additional factor is the presence of a sub-equatorial current through the Tethys Ocean and Panama seaway. This increased low-latitude connectivity helps prevent the development of salinity and $\delta^{18}O_{sw}$ gradients between the Atlantic and Pacific Oceans and is likely to be inhibiting the development of ocean overturning in the Atlantic. In the PI control simulation, the North Atlantic is about 1 ppt saltier than the North Pacific. In the Paleogene simulation, this gradient is reversed. Despite the increase in P-E+R over the Southern Ocean in the Paleogene simulation (mostly due to increased river runoff), salinities and $\delta^{18}O_{sw}$ in this region are increased. This increase is associated with increased advection of salt and $H_2^{18}O$ from the sub-tropics by a strong (>35 Sv) meridional overturning cell

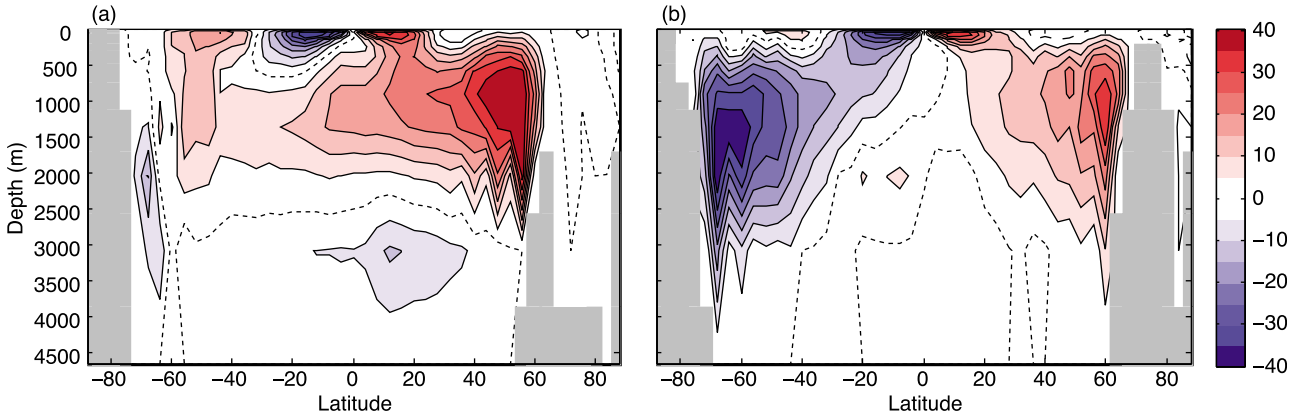

Figure 8. Global meridional overturning stream functions in Sverdrups (Sv) for (a) the preindustrial simulation and (b) the Paleogene simulation.

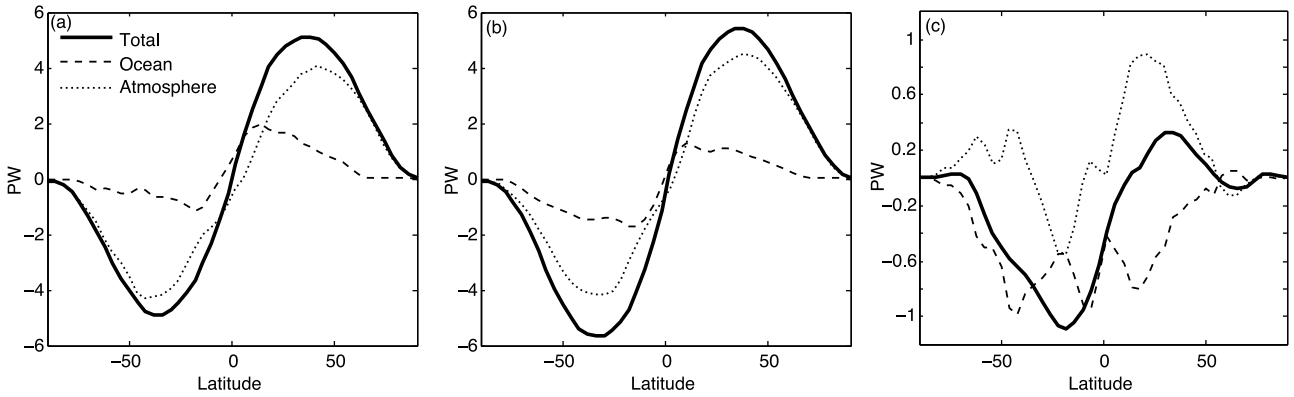

Figure 9. Northward heat transport in (a) the preindustrial simulation and (b) the Paleogene simulation. (c) Difference in northward heat transport (Paleogene–Preindustrial).

with an additional contribution from less negative precipitation-δ^{18}O over the Southern Ocean. In the equatorial regions surrounding South America, Africa, India and Asia, lower salinities and more negative surface ocean $\delta^{18}O_{sw}$ are related to high rates of atmospheric moisture convergence and significant volumes of river runoff into the coastal oceans. The discharge from large rivers results in steep horizontal $\delta^{18}O_{sw}$ gradients of up to 1.2 ‰ between adjacent grid-boxes. Despite a much higher freshwater input at the ocean surface, $\delta^{18}O_{sw}$ in the western (150–180°E) equatorial Pacific is increased. This increase is associated with increased advection of salt and $H_2^{18}O$ by a strong westward equatorial current and precipitation which has an isotopic composition similar to seawater (−5 to 0 ‰).

[23] Figure 11 shows the differences in surface ocean $\delta^{18}O_{sw}$ in the Paleogene and PI simulations converted into differences in δ^{18}O-based paleotemperature calculated using a calcite δ^{18}O value of −1 ‰. In regions where $\delta^{18}O_{sw}$ is higher in the Paleogene simulation, the impact is to increase δ^{18}O-derived Paleogene temperature estimates. The equations used to estimate temperature from $\delta^{18}O_c$ all have approximately linear trends for the range of temperatures typical of seawater [*Bemis et al.*, 1998]. This means that calculated difference in temperature for two different estimates of $\delta^{18}O_{sw}$ is relatively insensitive to the chosen value of $\delta^{18}O_c$.

[24] The majority of sites from which Paleogene carbonate δ^{18}O have been recovered are located in the equatorial Pacific Ocean, the Southern Ocean, the South Atlantic Ocean, and the Indian Ocean. For these locations, the impact of using the Paleogene $\delta^{18}O_{sw}$ distribution from ModelE-R would be to reduce meridional temperature gradient estimates for the early Paleogene. For example, for a meridional section through the South Atlantic, the temperature difference between the equator and the Southern Ocean is about 6°C less when simulated Paleogene $\delta^{18}O_{sw}$ is used rather than PI values. For this reason, the use of simulated estimates of Paleogene $\delta^{18}O_{sw}$ from ModelE-R does not reconcile modeled and published ($\delta^{18}O_c$-based) estimates of latitudinal temperature gradients. However, we note that there are significant uncertainties associated with simulations of Paleogene climate (including the uncertainty in the applied boundary conditions and deficiencies in the models; see section 5). Additionally, in many regions the Paleogene

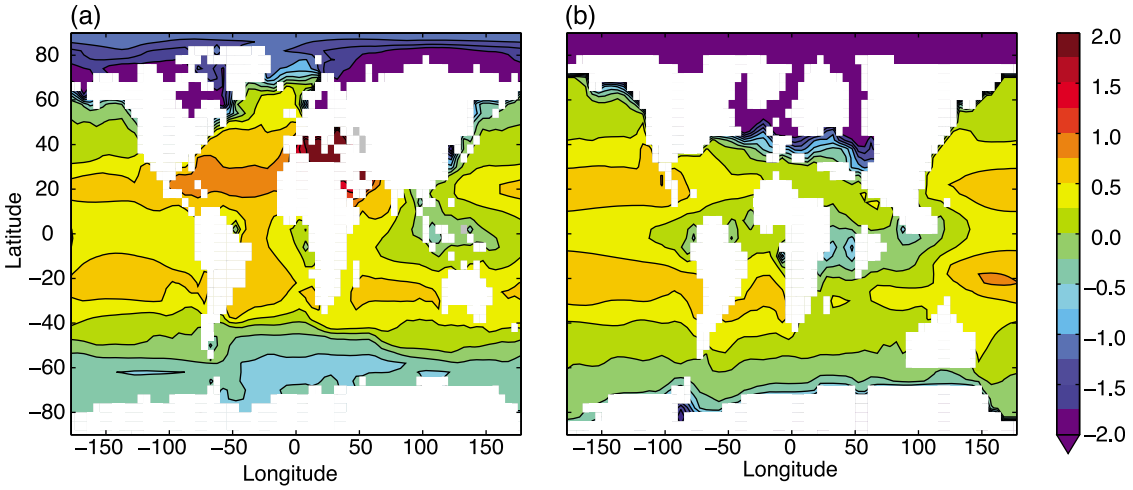

Figure 10. Maps of surface ocean $\delta^{18}O_{sw}$ (per mil vs VSMOW) from (a) the preindustrial simulation and (b) an early Paleogene simulation with GISS ModelE-R. Paleogene values are adjusted to have a global mean $\delta^{18}O_{sw}$ of zero to allow comparison with modern values.

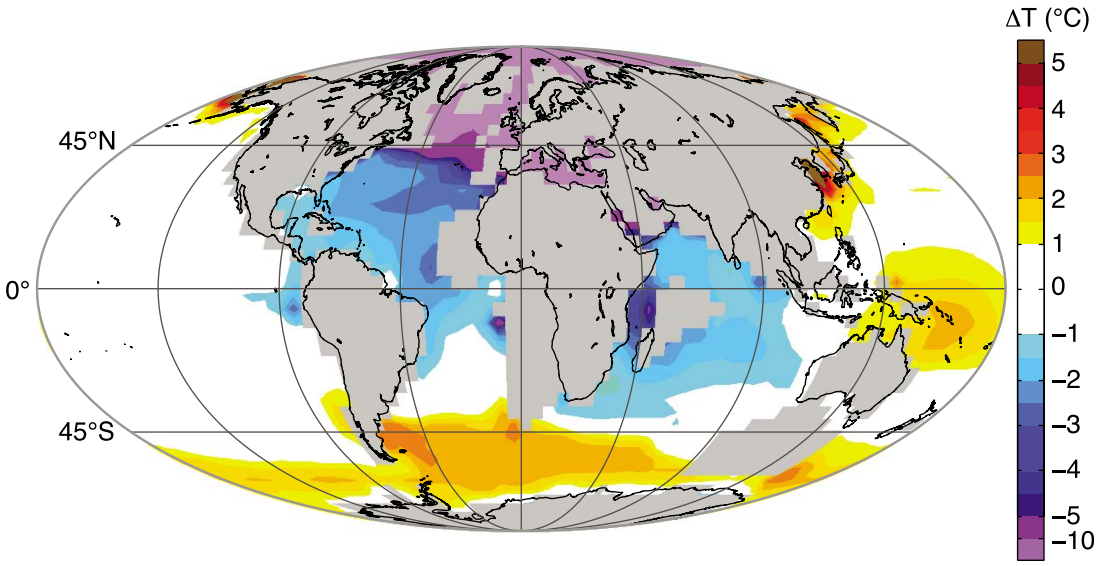

Figure 11. Difference in δ^{18}O-based paleotemperature estimates when simulated Paleogene $\delta^{18}O_{sw}$ values are used instead of $\delta^{18}O_{sw}$ values from the PI simulation. Paleogene values are adjusted to have a global mean $\delta^{18}O_{sw}$ of zero to allow comparison with modern values. Locations that are land in either simulation are masked in gray, and regions where the differences in estimated temperature are less than ±1°C are masked in white.

ocean basins are not aligned with their modern counterparts. For these reasons, the estimated impacts on paleotemperature estimates shown in Figure 11 should be interpreted with caution. However, these results demonstrate the potential sensitivity of paleotemperature estimates to the evolving distribution of $\delta^{18}O_{sw}$ in the oceans. Estimates of δ^{18}O-derived paleotemperature in the North Atlantic, Arctic, and Mediterranean/Tethys basins may be particularly sensitive to changes in paleogeography.

4. Model-Data Comparisons

4.1. Comparisons With Climate Proxies

[25] Results from the early Paleogene simulation with ModelE-R compare favorably with terrestrial climate reconstructions from 65 to 45 Ma, especially with data from the midlatitudes (Figure 12). However, the Paleogene simulation produces low (0–5°C) mean annual temperatures (MATs) in the Arctic, whereas terrestrial proxy data with paleolatitudes >78°N indicate MATs of >10°C (Figure 12a) and above freezing temperatures throughout the polar night (Figure 12b). Although pole-to-equator SST gradients are reduced in the Paleogene simulation relative to the PI control (Figure 2), meridional temperature gradients are not as low as those suggested by marine proxies (Figure 13). Figure 13 shows simulated Paleogene SSTs overlain with proxy temperature estimates from four time intervals. Data from the Paleocene-Eocene thermal maximum are excluded from the comparison and the sources of proxy data in Figure 13 are listed in Table S1.[1] In the low- and midlatitudes, model estimated SSTs compare favorably with proxy estimates. However, in the South Pacific and Arctic in particular, proxy SST estimates are much higher than those simulated. Simulated Paleogene temperatures in the abyssal ocean are 10–12°C and reflect winter SSTs between 65°S and 75°S. These values are in agreement with deep ocean temperatures derived from Mg/Ca analyses of early Eocene

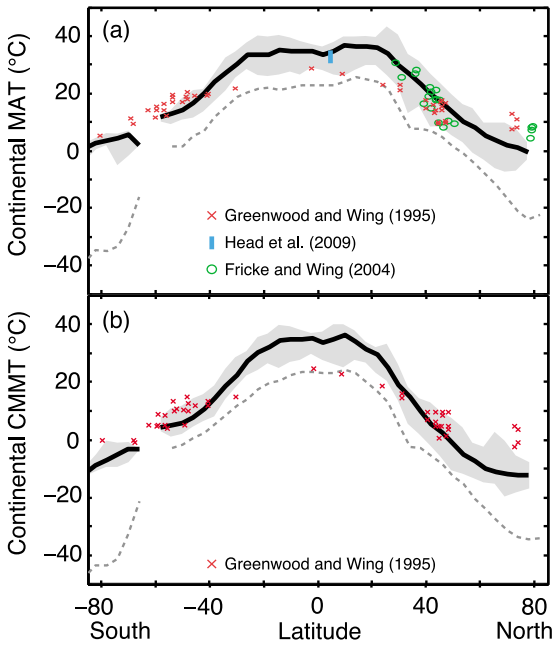

Figure 12. (a) Zonal mean continental mean annual surface air temperature (MAT) from the preindustrial simulation (dashed line) and Paleogene simulation (solid line) compared with terrestrial proxy data from the early Paleogene. (b) Zonal mean continental cold month mean temperature (CMMT), same legend as (a). Grey areas indicate the range of values used to calculate zonal means in the Paleogene simulation.

[1]Auxiliary materials are available in the HTML. doi:10.1029/2010PA002025.

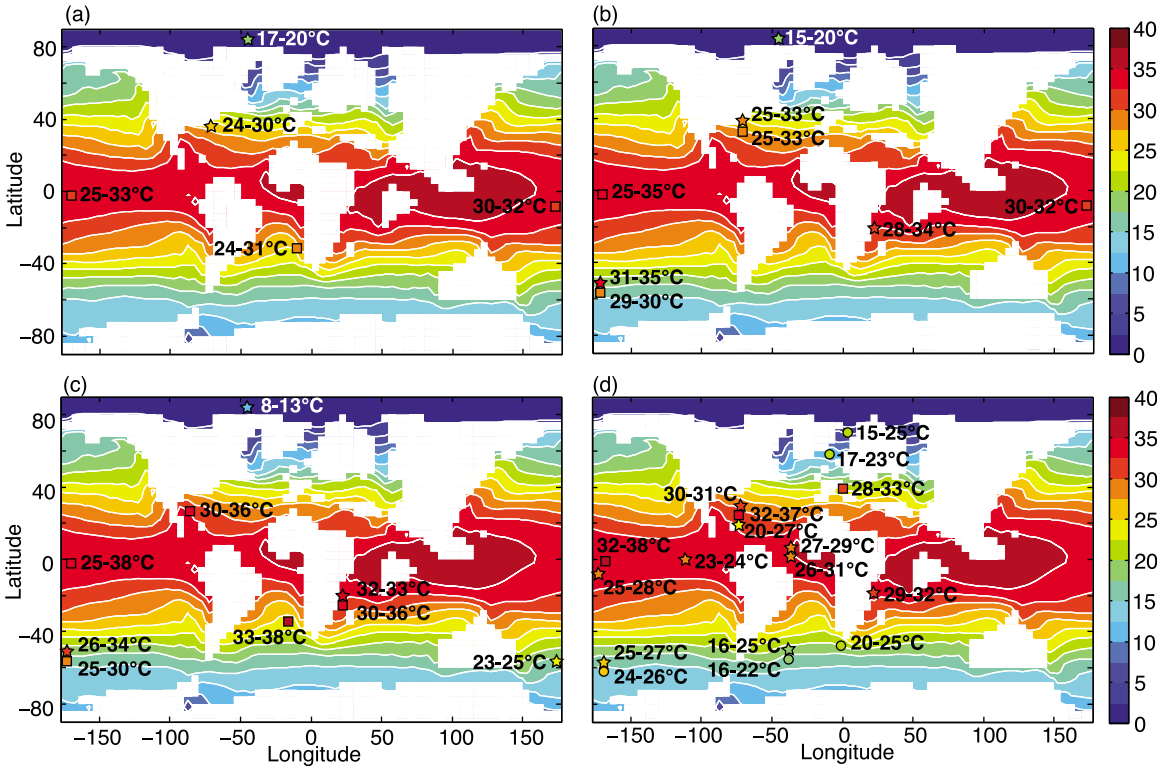

Figure 13. Mean annual sea-surface temperatures (°C) from the Paleogene simulation (contoured maps on all plots) compared with data from following marine temperature proxies: Mg/Ca of foraminiferal calcite (squares), the TEX_{86} index (stars) and the U^{K}_{37} alkenone unsaturation index (circles). The intervals plotted are (a) late Paleocene (59–56 Ma), (b) early Eocene (55–49 Ma), (c) middle Eocene (49–40 Ma) and (d) late Eocene (40–34 Ma).

age benthic foraminifera [*Lear et al.*, 2000; *Billups and Schrag*, 2003; *Tripati and Elderfield*, 2005]. Despite the agreement between proxy and simulated estimates of deep ocean temperature in southern hemisphere, simulated SSTs in the Southern Ocean are much lower than the very high SST temperatures estimated using TEX_{86} and planktic foraminiferal Mg/Ca analyses [e.g., *Burgess et al.*, 2008; *Hollis et al.*, 2009]. If the South Pacific SST estimates from proxy data are accurate, the mechanism(s) responsible for such warmth remain unclear as it seems unlikely that ocean overturning or gyral circulation could be sufficiently vigorous to reduce temperature gradients so dramatically.

4.2. Comparison With Fossil δ^{18}O

[26] Modeled temperatures and $\delta^{18}O_{sw}$ were converted into estimates of equilibrium $\delta^{18}O_c$ using an equation $(T(°C) = 16.1 - 4.64 \cdot (\delta^{18}O_c - \delta^{18}O_{sw}) + 0.09 \cdot (\delta^{18}O_c - \delta^{18}O_{sw})^2)$ derived from a laboratory study of inorganic carbonates [*Kim and O'Neil*, 1997] and assuming a global mean $\delta^{18}O_{sw}$ value of −0.81 ‰. The range of abyssal ocean $\delta^{18}O_c$ from the Paleogene (3–4 ‰) and PI (0–1 ‰) simulations are in good agreement with benthic foraminiferal $\delta^{18}O_c$ from the early Paleogene and the Holocene, respectively [*Zachos et al.*, 2001, 2008]. This comparison, along with independent estimates of Paleogene deep ocean temperatures, suggests that the Paleogene simulation is accurately reproducing deep ocean temperatures and $\delta^{18}O_{sw}$.

[27] Figure 14 shows simulated $\delta^{18}O_c$ from a model depth of 43.5 m overlain with $\delta^{18}O_c$ from Paleogene planktic foraminifera and molluscs. Values from this depth are appropriate for comparison with $\delta^{18}O_c$ measurements from mixed-layer dwelling foraminifera. For example, the modern mixed-layer species *Globigerinoides ruber* (pink) is most abundant in the upper 0–50 m of the water column in the North Atlantic [*Wilke et al.*, 2009]. Data from the Paleocene-Eocene thermal maximum are excluded from the comparisons and, for each site, the most negative fossil $\delta^{18}O_c$ is plotted. The sources of $\delta^{18}O_c$ data used in the comparisons are listed in Table S1. The comparisons in Figure 14 show that, in almost all low- and midlatitude locations, fossil $\delta^{18}O_c$ data are 1–3 ‰ heavier than simulated mixed-layer $\delta^{18}O_c$. In contrast, fossil $\delta^{18}O_c$ compares favorably with simulated $\delta^{18}O_c$ in the high-latitudes.

[28] As was noted earlier, it is possible that some of the mismatch between simulated and fossil $\delta^{18}O_c$ is a result of the inaccurate prescription of global mean $\delta^{18}O_{sw}$. However, reversing the apparent agreement in the high latitudes and disagreement in the low latitudes would require global mean $\delta^{18}O_{sw}$ to be 2–3 ‰ higher. A change of this magnitude would require the storage of very large volume of isotopically light water on the continents (equivalent to ~2.5–3.7 times as much ice as is currently stored on the continents). Changing global mean $\delta^{18}O_{sw}$ to improve the agreement with fossil $\delta^{18}O_c$ recovered from low-latitude open-ocean

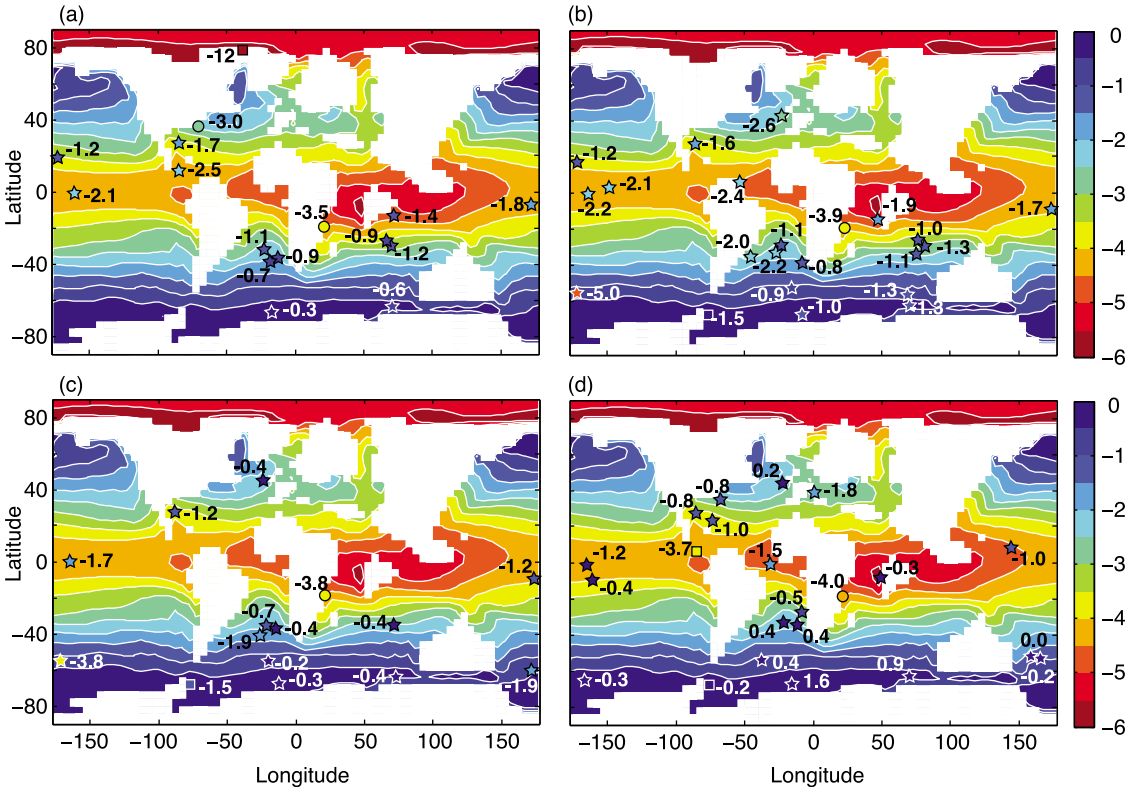

Figure 14. Paleogene $\delta^{18}O_c$ (per mil vs VPDB) calculated from simulated temperatures and $\delta^{18}O_{sw}$ from a model depth of 43.5 m (contoured maps on all plots). Simulated values are compared with fossil $\delta^{18}O_c$ data from open-ocean planktic foraminifera (stars), 'glassy' foraminifera (circles), and molluscs (squares) from the following time intervals: (a) the late Paleocene (59–56 Ma), (b) the early Eocene (55–49 Ma), (c) the middle Eocene (49–40 Ma), and (d) the late Eocene (40–34 Ma).

sites would also reduce the agreement with fossil $\delta^{18}O_c$ from deep ocean and well preserved surface ocean foraminifera.

[29] Figures 13 and 14 show that, generally speaking, simulated and fossil $\delta^{18}O_c$ data are in agreement pole wards of ~40° latitude, whereas simulated and proxy estimates of ocean temperature are in agreement between ~40° latitude and the equator. There are several ways to interpret this apparent inconsistency in the high latitudes: (1) The high latitude fossil $\delta^{18}O_c$ measurements are recording equilibrium values, indicating accurate simulation of surface temperatures and $\delta^{18}O_{sw}$. Implicit in this conclusion is that the very warm temperature estimates from the other proxies are wrong. (2) The high latitude $\delta^{18}O_c$ data are biased to an unknown extent by nonequilibrium or diagenetic processes meaning that the apparent agreement with simulated temperature and $\delta^{18}O_{sw}$ is of little value for the constraint of surface conditions in the high latitudes. (3) The high latitude fossil $\delta^{18}O_c$ measurements are recording equilibrium values, but the agreement with simulated values is a result of compensating errors in the simulation of $\delta^{18}O_{sw}$ and temperature. Unfortunately, this comparison is hampered by the lack of co-located measurements of $\delta^{18}O_c$ and other ocean temperature proxies, especially in locations where the simulated and estimated temperatures disagree the most (e.g., the Arctic). Nevertheless, in some locations (e.g., the south Pacific during the early to middle Eocene) very high temperature estimates from temperature proxies are consistent with very negative $\delta^{18}O_c$ measurements (and both disagree with simulated values). In this particular case, it is unknown what ocean-atmosphere processes might be missing from models that could sustain similar temperatures at the equator and at ~55°S.

5. Discussion

5.1. Complications in the Interpretation of Fossil Carbonate $\delta^{18}O$

[30] It is possible that fossil carbonates plotted in Figure 14 are not recording equilibrium $\delta^{18}O$ representative of the surface ocean. For example, none of the foraminiferal genera (e.g., *Morozovella*, *Acarinina*) assumed to inhabit the surface layers of the ocean during the Paleogene are extant, so it is impossible to know definitively whether the values recorded by their tests are true equilibrium values. It is well-known from studies of modern planktic foraminifera that 'vital effects' of 0.5–1.0 ‰ can be expressed both within and between species [e.g., *Bemis et al.*, 1998]. The origin of these 'vital effects' may be a result of kinetic discrimination of heavier isotopes during the biological precipitation of carbonate, differences between ambient seawater chemistry and the fluid chemistry at the site of calcification, or other metabolic effects [e.g., *McConnaughey*, 1989a, 1989b; *Wefer and Berger*, 1991; *Zeebe*, 2007]. Another uncertainty is the paleo-depth inhabited by extinct species of foraminifera. The paleoecology of Paleogene planktic foraminifera is usually inferred from inter-species $\delta^{18}O$-$\delta^{13}C$ relation-

ships [e.g., *Pearson et al.*, 1993]. For this reason, the depths at which Paleogene foraminifera calcified remain uncertain. In addition, the average $\delta^{18}O$ composition of Paleogene foraminiferal tests likely reflects precipitation over a range of temperatures and $\delta^{18}O_{sw}$ values [*Schmidt and Mulitza*, 2002].

[31] Previous studies have also suggested that Paleogene foraminifera recovered from ocean open sites may have undergone diagenetic alteration, which would cause them to have $\delta^{18}O_c$ biased toward benthic values [e.g., *Schrag*, 1999; *Pearson et al.*, 2001; *Sexton et al.*, 2006; *Pearson et al.*, 2007;]. For example, *Pearson et al.* [2001] showed that exceptionally well preserved 'glassy' foraminifera recovered from hemipelagic clays in Tanzania are as much as 4 ‰ lighter than foraminifera of a similar age and from a similar latitude recovered from an open-ocean site. This hypothesis of diagenetic alteration of open-ocean samples is supported by scanning electron micrographs of Eocene planktic foraminifera that show evidence for recrystallization [*Sexton et al.*, 2006]. However, the extent of recrystallization and the amount of secondary calcite present is the subject of debate [*Pearson et al.*, 2001; *Tripati et al.*, 2003]. The comparisons in Figure 14 are consistent with the suggestion that Paleogene planktic foraminifera from open-ocean sites have undergone some recrystallization. This hypothesis could account for both the mismatch in the low- and midlatitudes and the observed agreement in the high-latitudes (where the differences between benthic and planktic $\delta^{18}O_c$ are much lower). We also find good agreement between simulated and fossil $\delta^{18}O_c$ for 'glassy' foraminiferal carbonate from Tanzania [*Pearson et al.*, 2001; *Pearson et al.*, 2007] and 'porcelain' foraminiferal carbonate from New Jersey [*Zachos et al.*, 2006].

[32] An additional factor that our simulated $\delta^{18}O_c$ estimates in Figure 14 do not take into account is the impact of lower seawater pH on equilibrium calcite $\delta^{18}O$. *Spero et al.* [1997] demonstrated a carbonate ion effect on oxygen (and carbon) isotope fractionation in planktic foraminiferal carbonates. To explain this effect, *Zeebe* [1999, 2001] hypothesized that reduced surface ocean pH (which drives a reduced carbonate/bicarbonate ion ratio in seawater) during high CO_2 intervals could be responsible for equilibrium calcite that is less negative than calcite synthesized from seawater under low CO_2 conditions. For example, an increase of atmospheric CO_2 from 280 ppm to 1200 ppm would reduce the concentration of surface ocean CO_3^{2-} by ~50–150 μmol/kg, depending on the corresponding changes in ocean alkalinity. These changes in CO_3^{2-}, combined with a $\delta^{18}O$ vs CO_3^{2-} slope of between −0.002 and −0.005‰ $(\mu mol/kg)^{-1}$ [*Spero et al.*, 1997], suggest that the pH/carbonate ion effect may be responsible for 0.1–0.8 ‰ of the observed discrepancy.

5.2. Uncertainty in Paleoclimate Model Simulations

[33] The error in model simulations of ancient climates can be divided into two broad categories: 'model error', which exists because models are simplified representations of the climate system and 'boundary condition error', which arises from uncertainties in the applied boundary conditions. Model error can arise as a result of inaccurate model physics/dynamics (e.g., physical parameterizations and the assumptions made to reduce the complexity of the underlying equations) or unmodelled processes (e.g., vegetation feedbacks). Examples of these types of uncertainty include, the numerical approximations used to describe the equations of fluid flow, the limited spatial resolution of climate models and the inaccurate parameterization of unresolved physical and dynamic processes. ModelE-R has a performance that is typical of the other coupled models used in the most recent IPCC inter-comparisons [*Randall et al.*, 2007]. Deficiencies in simulations with ModelE-R of the modern climate system include weak east-west SST gradients in the tropics, shallow deep-water formation in the North Atlantic, and weak ocean-atmosphere variability in the tropics [*Hansen et al.*, 2007].

[34] There is no doubt that some of the mismatch between simulated and foraminiferal $\delta^{18}O_c$ values is a result of the inaccurate response of ocean temperatures and $\delta^{18}O_{sw}$ in ModelE-R to the prescribed Paleogene boundary conditions due to the existing biases in the physical model. However, it is arguable that a much larger source of error in our Paleogene simulation is a result of the uncertainty in the applied boundary conditions (e.g., greenhouse gas concentrations, land-sea distribution, vegetation). Although the effect of these boundary condition uncertainties on simulations of Paleogene climate are poorly characterized, results from previous sensitivity studies suggest that the impacts on regional and global climate, and consequently on $\delta^{18}O_{sw}$, could be very large.

[35] The details of global paleogeography and the geometry and bathymetry of the Paleogene ocean are particularly uncertain and a previous sensitivity study has demonstrated the strong sensitivity of regional salinity and $\delta^{18}O_{sw}$ to relatively small changes in Paleogene bathymetry [*Roberts et al.*, 2009]. The position of shorelines and the depth and width of narrow ocean gateways during the early Paleogene [e.g., *Rogl*, 1999; *Eagles et al.*, 2006; *Scher and Martin*, 2006; *Akhmetiev and Beniamovski*, 2009] are especially uncertain because they are sensitive to both local tectonics and changes in global sea level. Previous studies have demonstrated that changes to the position of solid boundaries in the ocean can have a significant impact on patterns of surface ocean circulation, heat transport, and the location and magnitude of deep-water formation [*Barron and Peterson*, 1991; *Bice et al.*, 1998; *Crowley*, 1998; *Toggweiler and Bjornsson*, 2000; *Roberts et al.*, 2009]. In particular, the presence or absence of north-south oriented barriers, such as the Drake Passage, are known to strongly affect meridional overturning circulation, the development of ocean gyres, the equatorward extent of sea-ice, and the intensity of poleward ocean heat transport [*Smith et al.*, 2006; *Marshall et al.*, 2007; *Enderton and Marshall*, 2009].

[36] For the reasons outlined above, uncertainties in paleogeography, the position of continental drainage boundaries, and the configuration of shallow seaways are arguably the leading sources of uncertainty in modeled estimates of spatial gradients of Paleogene $\delta^{18}O_{sw}$. These factors all have the potential to influence the redistribution of freshwater and ^{18}O both within and between ocean basins in ways that are not easily predictable due to the nonlinear nature of the ocean system and the existence of thresholds such as presence/absence of ocean gateways. In contrast, although proxy-based estimates of atmospheric CO_2 concentrations during the early Paleogene range from 500 to 3500 ppmv [e.g.,

Pagani et al., 2005; *Pearson and Palmer*, 2000; *Royer*, 2006], the response of $\delta^{18}O_{sw}$ is potentially more predictable due to the very zonal way in which atmospheric moisture convergence responds to global warming.

[37] Other uncertainties which could impact model-based estimates of $\delta^{18}O_{sw}$ are outlined below. The preservational biases in proxy and fossil records means that the gridded global fields used as model boundary conditions (e.g., topography and vegetation) are inevitably under-determined. Model sensitivity studies suggest that uncertainties in vegetation and topographic boundary conditions have the potential to affect $\delta^{18}O_{sw}$ via the hydrological cycle (through large impacts on land-surface temperatures, precipitation and patterns of atmospheric circulation), particularly at regional/local scales [e.g., *Shukla and Mintz*, 1982; *Sud et al.*, 1988; *Crowley*, 1998, *Fraedrich et al.*, 1999; *Sewall et al.*, 2000; *Lunt et al.*, 2010]. The uncertainty in Paleogene mean ocean salinity [*Hay et al.*, 2006] could also have an impact on the spatial gradients of $\delta^{18}O_{sw}$. The nonlinearity of the equation of state for means that changes to the average ocean salinity could potentially affect a variety of processes such as open ocean convection, geostrophic transports, and the structure of areas of shallow stratification such as the tropical warm pool. The impact of changes in global mean ocean salinity on meridional gradients in the ocean is a topic that has yet to be explored with an isotope-enabled climate model and could form the basis of a future study.

5.3. High Latitude Temperatures

[38] Mismatch between proxy- and model-based estimates of high latitude temperatures is a feature of previous coupled modeling studies of the early Paleogene [e.g., *Huber and Sloan*, 2001] and could be due to deficiencies in the model simulations (see above), uncertainties in the interpretation of the proxies, or unaccounted for feedback processes that preferentially warm the poles. An additional uncertainty is the low temporal and spatial resolution of geological proxy-data used to validate climate model simulations. For example, model simulations represent a climate 'snapshot' for a particular combination of boundary conditions, whereas compilations of proxy data typically represent a large window of geological time, which may be sampling a variety of climatic conditions. High-latitude proxy data also generally reflect a bias toward warm-season temperatures and do not usually record annual average conditions.

[39] Despite the potential for significant uncertainty in the interpretation of temperature proxies, there is a large body of evidence for year-round warmth in the Arctic during the early Paleogene [e.g., *Brinkhuis et al.*, 2006; *Fricke and Wing*, 2004; *Greenwood and Wing*, 1995; *Jahren*, 2007]. If the proxy reconstructions which indicate reduced latitudinal temperature gradients during the Paleogene are accurate, this mismatch between models and data could be due to (1) the inadequately constrained model boundary conditions or (2) a missing feedback process that might have preferentially warmed the high latitudes or reduced tropical climate sensitivity to greenhouse gases. Previously suggested mechanisms for reduced meridional temperature gradients include (1) high-latitude cloud feedbacks [*Abbot et al.*, 2009; *Abbot and Tziperman*, 2008; *Sloan et al.*, 1992], (2) increased ocean mixing driven by tropical cyclones [*Korty et al.*, 2008], (3) changes to global heat transport [*Huber and Sloan*, 1999], and (4) an increased pole ward heat flux associated with the propagation of atmospheric Rossby waves from low- to high-latitudes driven by the presence of an ocean warm pool and the resulting zonal asymmetries in tropical convection [*Lee et al.*, 2011]. However, some of these hypotheses (e.g., increased ocean heat transport) have been shown to be unlikely [*Huber and Sloan*, 2001]. The mechanism postulated by *Lee et al.* [2011] suggests that ModelE-R might be more prone to 'equable' climates if it did not have a bias toward weak east-west SST gradients in the tropics [*Hansen et al.*, 2007; *Schmidt et al.*, 2007].

5.4. Comparison With Results From Another Isotope-Enabled Climate Model

[40] Three other studies have used climate models to simulate the impact of 'greenhouse' conditions on seawater $\delta^{18}O_{sw}$ [*Roche et al.*, 2006; *Tindall et al.*, 2010; *Zhou et al.*, 2008], and only *Tindall et al.* [2010] used a model configuration that was comparable to the Paleogene configuration of ModelE-R. *Tindall et al.* [2010] used an isotope-enabled version of HadCM3 configured with a new (proprietary) Eocene paleogeography and 6 × preindustrial CO_2 to simulate early Eocene $\delta^{18}O_{sw}$. Despite the higher greenhouse gas concentrations used by *Tindall et al.* [2010], and the slightly higher climate sensitivity of HadCM3 (ΔT_{2xCO2} = 3.3°C), the global mean SST increase is similar in both models (10°C in HadCM3 and 9°C in ModelE-R). This suggests that non-greenhouse gas warming in the Paleogene simulation with ModelE-R is higher than in the Eocene simulation with HadCM3.

[41] Estimates of early Paleogene $\delta^{18}O_c$ from ModelE-R and HadCM3 [*Tindall et al.*, 2010] are both broadly consistent with the hypothesis that early Paleogene open-ocean foraminifera from the mid- and low-latitudes have undergone diagenetic alteration. However, on closer inspection, there are large differences in the spatial distributions of Paleogene $\delta^{18}O_{sw}$. For example, results from HadCM3 suggest that, during the early Eocene, surface $\delta^{18}O_{sw}$ values in the North Atlantic and the southern Indian Ocean were higher than modern values and that surface $\delta^{18}O_{sw}$ values in the Southern Ocean were lower than modern values. This is in direct contrast to the results from ModelE-R (see Figure 10). Some of the $\delta^{18}O_{sw}$ discrepancy in the North Atlantic is reduced when the results from HadCM3 are compared to a Paleogene configuration of ModelE-R which, like the HadCM3 configuration, does not allow flow through the Greenland-Norway seaway [*Roberts et al.*, 2009]. However, most of the differences in simulated $\delta^{18}O_{sw}$ remain, and the changes in the subtropical North Atlantic relative to the PI control inferred from HadCM3 and ModelE-R are still of opposite signs.

[42] In some regions, the differences in simulated Paleogene $\delta^{18}O_{sw}$ result in different conclusions regarding the re-evaluation of $\delta^{18}O_c$-based estimates of SST. For example, *Pearson et al.* [2007] estimated early Eocene SSTs from coastal Tanzania of ~33°C using a $\delta^{18}O_{sw}$ value of −0.5 ‰. When a value of −1.0 ‰ is used instead (the simulated value from ModelE-R from a depth of 43.5 m), the estimated temperatures are reduced to ~30°C. In contrast, *Tindall et al.* [2010] used simulated Eocene $\delta^{18}O_{sw}$

from HadCM3 to estimate higher (+2–3°C) Paleogene temperatures from Tanzania. Ultimately, these inconsistencies are a result of the respective model biases and the differences in the applied boundary conditions. However, each model simulation provides a 'best guess' of early Paleogene $\delta^{18}O_{sw}$ given the available constraints. The differing results emphasize the sensitivity of $\delta^{18}O_{sw}$ to climatic and tectonic boundary conditions. For this reason, the uncertainties in regional Paleogene $\delta^{18}O_{sw}$, and hence $\delta^{18}O$-based estimates of paleotemperature, are probably much larger than is commonly assumed.

6. Conclusions

[43] If proxy constraints are unavailable, forward modeling studies are the only way to make independent estimates of the spatial gradients of $\delta^{18}O_{sw}$ in ancient oceans. The results from two simulations with a water isotope-enabled GCM (GISS ModelE-R) indicate that surface ocean gradients of $\delta^{18}O_{sw}$ during the early Paleogene could have been very different to those in the modern ocean. The changes in $\delta^{18}O_{sw}$ inferred from ModelE-R are sufficient to bias carbonate $\delta^{18}O$ paleotemperature estimates in large parts of the ocean by more than ±2°C. However, some of the changes in $\delta^{18}O_{sw}$ inferred from ModelE-R are in direct contrast with those from another isotope-enabled model [*Tindall et al.*, 2010] which used different, but equally plausible, Paleogene boundary conditions. These results suggest that there is significant uncertainty in the spatial gradients of Paleogene $\delta^{18}O_{sw}$ due to uncertainties in the applied model boundary conditions (particularly the geometry of ocean basins). For this reason, Paleogene SST estimates derived from carbonate $\delta^{18}O$ may have much larger uncertainties than have previously been assumed. Isolation of the processes most responsible for the differences in simulated $\delta^{18}O_{sw}$ will require further model intercomparison work and, ideally, additional sensitivity simulations using common forcings and boundary conditions across multiple models.

[44] **Acknowledgments.** We thank NASA GISS for institutional support. A.N.L. was supported by NSF ATM 07-53868, C.D.R. was supported by a NERC studentship (NER/S/A/2006/14070), and A.K.T. was supported by the UCLA Division of Physical Sciences, NERC, and Magdalene College. We thank an anonymous reviewer and G.A. Schmidt for helpful comments on previous versions of this work and K. Bice and J. Sewall for providing us with gridded data for the model boundary conditions.

References

Abbot, D. S., and E. Tziperman (2008), Sea ice, high-latitude convection, and equable climates, *Geophys. Res. Lett.*, L03702, doi:10.1029/2007GL032286.

Abbot, D. S., M. Huber, G. Bousquet, and C. C. Walker (2009), High-CO_2 cloud radiative forcing feedback over both land and ocean in a global climate model, *Geophys. Res. Lett.*, *36*, L05702, doi:10.1029/2008GL036703.

Akhmetiev, M. A., and V. N. Beniamovski (2009), Paleogene floral assemblages around epicontinental seas and straits in Northern Central Eurasia: Proxies for climatic and paleogeographic evolution, *Geol. Acta*, *7*(1–2), 297–309.

Aleinov, I., and G. A. Schmidt (2006), Water isotopes in the GISS ModelE land surface scheme, *Global Planet. Change*, *51*(1–2), 108–120, doi:10.1016/j.gloplacha.2005.12.010.

Barron, E., and W. Peterson (1991), The Cenozoic ocean circulation based on ocean General Circulation Model results, *Palaeogeogr. Palaeoclimatol. Palaeoecol.*, *83*(1–3), 1–28, doi:10.1016/0031-0182(91)90073-Z.

Bartdorff, O., K. Wallmann, M. Latif, and V. Semenov (2008), Phanerozoic evolution of atmospheric methane, *Global Biogeochem. Cycles*, *22*, GB1008, doi:10.1029/2007GB002985.

Beerling, D., R. A. Berner, F. T. Mackenzie, M. B. Harfoot, and J. A. Pyle (2009), Methane and the CH_4-related greenhouse effect over the past 400 million years, *Am. J. Sci.*, *309*, 97–113, doi:10.2475/02.2009.01.

Bemis, B. E., H. J. Spero, J. Bijma, and D. W. Lea (1998), Reevaluation of the oxygen isotopic composition of planktonic foraminifera: Experimental results and revised paleotemperature equations, *Paleoceanography*, *13*(2), 150–160, doi:10.1029/98PA00070.

Bice, K. L., and J. Marotzke (2002), Could changing ocean circulation have destabilized methane hydrate at the Paleocene/Eocene boundary?, *Paleoceanography*, *17*(2), 1018, doi:10.1029/2001PA000678.

Bice, K. L., E. J. Barron, and W. H. Peterson (1998), Reconstruction of realistic Early Eocene paleobathymetry and ocean GCM sensitivity to specified basin configuration, in *Tectonic Boundary Conditions for Climate Reconstructions*, edited by T. J. Crowley and K. C. Burke, pp. 327–350, Oxford Univ. Press, New York.

Bice, K., C. Scotese, D. Seidov, and E. Barron (2000), Quantifying the role of geographic change in Cenozoic ocean heat transport using uncoupled atmosphere and ocean models, *Palaeogeogr. Palaeoclimatol. Palaeoecol.*, *161*, 295–310, doi:10.1016/S0031-0182(00)00072-9.

Bigg, G. R., and E. J. Rohling (2000), An oxygen isotope data set for marine water, *J. Geophys. Res.*, *105*, 8527–8535, doi:10.1029/2000JC900005.

Bijl, P. K., S. Schouten, A. Sluijs, G. J. Reichart, J. C. Zachos, and H. Brinkhuis (2009), Early Palaeogene temperature evolution of the southwest Pacific Ocean, *Nature*, *461*, 776–779, doi:10.1038/nature08399.

Billups, K., and D. P. Schrag (2003), Application of benthic foraminiferal Mg/Ca ratios to questions of Cenozoic climate change, *Earth Planet. Sci. Lett.*, *209*(1–2), 181–195, doi:10.1016/S0012-821X(03)00067-0.

Brinkhuis, H., et al. (2006), Episodic fresh surface waters in the Eocene Arctic Ocean, *Nature*, *441*, 606–609, doi:10.1038/nature04692.

Burgess, C. E., P. N. Pearson, C. H. Lear, H. E. G. Morgans, L. Handley, R. D. Pancost, and S. Schouten (2008), Middle Eocene climate cyclicity in the southern Pacific: Implications for global ice volume, *Geology*, *36*(8), 651–654, doi:10.1130/G24762A.1.

Craig, H., and L. I. Gordon (1965), Deuterium and oxygen 18 variations in the ocean and the marine atmosphere, in *Stable Isotopes in Oceanographic Studies and Paleotemperatures*, edited by E. Tongiorgi, pp. 9–130, Lab. di Geol. Nucl., C. N. R., Pisa, Italy.

Crowley, T. J. (1998), Significance of tectonic boundary conditions for paleoclimate simulations, in *Tectonic Boundary Conditions for Climate Reconstructions*, edited by T. J. Crowley and K. C. Burke, pp. 3–17, Oxford Univ. Press, New York.

Eagles, G., R. Livermore, and P. Morris (2006), Small basins in the Scotia Sea: The Eocene Drake Passage gateway, *Earth Planet. Sci. Lett.*, *242*, 343–353, doi:10.1016/j.epsl.2005.11.060.

Emiliani, C. (1955), Pleistocene temperatures, *J. Geol.*, *63*(6), 538–578, doi:10.1086/626295.

Enderton, D., and J. Marshall (2009), Explorations of atmosphere-ocean-ice climates on an aquaplanet and their meridional energy transports, *J. Atmos. Sci.*, *66*(6), 1593–1611, doi:10.1175/2008JAS2680.1.

Fraedrich, K., A. Kleidon, and F. Lunkeit (1999), A green planet versus a desert world: Estimating the effect of vegetation extremes on the atmosphere, *J. Clim.*, *12*(10), 3156–3163, doi:10.1175/1520-0442(1999)012<3156:AGPVAD>2.0.CO;2.

Fricke, H. C., and S. L. Wing (2004), Oxygen isotope and paleobotanical estimates of temperature and $\delta^{18}O$-latitude gradients over North America during the early Eocene, *Am. J. Sci.*, *304*(7), 612–635, doi:10.2475/ajs.304.7.612.

Gent, P., and J. McWilliams (1990), Isopycnal mixing in ocean circulation models, *J. Phys. Oceanogr.*, *20*(1), 150–155, doi:10.1175/1520-0485(1990)020<0150:IMIOCM>2.0.CO;2.

Gent, P., J. Willebrand, T. McDougall, and J. McWilliams (1995), Parameterizing eddy-induced tracer transports in ocean circulation models, *J. Phys. Oceanogr.*, *25*(4), 463–474, doi:10.1175/1520-0485(1995)025<0463:PEITTI>2.0.CO;2.

Greenwood, D. R., and S. L. Wing (1995), Eocene continental climates and latitudinal temperature-gradients, *Geology*, *23*(11), 1044–1048, doi:10.1130/0091-7613(1995)023<1044:ECCALT>2.3.CO;2.

Griffies, S. (1998), The Gent-McWilliams skew flux, *J. Phys. Oceanogr.*, *28*(5), 831–841, doi:10.1175/1520-0485(1998)028<0831:TGMSF>2.0.CO;2.

Hansen, J., et al. (2007), Climate simulations for 1880–2003 with GISS modelE, *Clim. Dyn.*, *29*, 661–696, doi:10.1007/s00382-007-0255-8.

Hay, W. W., A. Migdisov, A. N. Balukhovsky, C. N. Wold, S. Flogel, and E. Soding (2006), Evaporites and the salinity of the ocean during the Phanerozoic: Implications for climate, ocean circulation and life,

Palaeogeogr. Palaeoclimatol. Palaeoecol., *240*(1–2), 3–46, doi:10.1016/j.palaeo.2006.03.044.

Head, J. J., J. I. Bloch, A. K. Hastings, J. R. Bourque, E. A. Cadena, F. A. Herrera, P. D. Polly, and C. A. Jaramillo (2009), Giant boid snake from the Palaeocene neotropics reveals hotter past equatorial temperatures, *Nature*, *457*, 715–717, doi:10.1038/nature07671.

Hollis, C. J., et al. (2009), Tropical sea temperatures in the high-latitude South Pacific during the Eocene, *Geology*, *37*(2), 99–102, doi:10.1130/G25200A.1.

Huber, M., and L. C. Sloan (1999), Warm climate transitions: A general circulation modeling study of the Late Paleocene thermal maximum (~56 Ma), *J. Geophys. Res.*, *104*(D14), 16,633–16,655, doi:10.1029/1999JD900272.

Huber, M., and L. C. Sloan (2001), Heat transport, deep waters, and thermal gradients: Coupled simulation of an Eocene Greenhouse Climate, *Geophys. Res. Lett.*, *28*(18), 3481–3484, doi:10.1029/2001GL012943.

Jahren, A. H. (2007), The Arctic Forest of the Middle Eocene, *Annu. Rev. Earth Planet. Sci.*, *35*, 509–540, doi:10.1146/annurev.earth.35.031306.140125.

Kim, S.-T., and J. R. O'Neil (1997), Equilibrium and non-equilibrium oxygen isotope effects in synthetic carbonates, *Geochim. Cosmochim. Acta*, *61*, 3461–3475, doi:10.1016/S0016-7037(97)00169-5.

Korty, R. L., K. A. Emanuel, and J. R. Scott (2008), Tropical cyclone-induced upper-ocean mixing and climate: Application to equable climates, *J. Clim.*, *21*(4), 638–654, doi:10.1175/2007JCLI1659.1.

Large, W., J. McWilliams, and S. Doney (1994), Oceanic vertical mixing: A review and a model with a nonlocal boundary layer parameterization, *Rev. Geophys.*, *32*(4), 363–404, doi:10.1029/94RG01872.

Laskar, J., P. Robutel, F. Joutel, M. Gastineau, A. C. M. Correia, and B. Levrard (2004), A long-term numerical solution for the insolation quantities of the Earth, *Astron. Astrophys.*, *428*(1), 261–285, doi:10.1051/0004-6361:20041335.

Lear, C. H., H. Elderfield, and P. A. Wilson (2000), Cenozoic deep-sea temperatures and global ice volumes from Mg/Ca in benthic foraminiferal calcite, *Science*, *287*, 269–272, doi:10.1126/science.287.5451.269.

Lee, S., S. Feldstein, D. Pollard, and T. White (2011), Do planetary wave dynamics contribute to equable climates?, *J. Clim.*, *24*, 2391–2404, doi:10.1175/2011JCLI3825.1.

LeGrande, A. N., and G. A. Schmidt (2006), Global gridded data set of the oxygen isotopic composition in seawater, *Geophys. Res. Lett.*, *33*, L12604, doi:10.1029/2006GL026011.

Levitus, S., R. Burgett, and T. Boyer (1994), *World Ocean Atlas 1994*, vol. 3, *Salinity, NOAA Atlas NESDIS*, vol. 3, 111 pp., NOAA, Silver Spring, Md.

Liu, J., G. Schmidt, D. Martinson, D. Rind, G. Russell, and X. Yuan (2003), Sensitivity of sea ice to physical parameterizations in the GISS global climate model, *J. Geophys. Res.*, *108*(C2), 3053, doi:10.1029/2001JC001167.

Lunt, D. J., A. M. Haywood, G. A. Schmidt, U. Salzmann, P. J. Valdes, and H. J. Dowsett (2010), Earth system sensitivity inferred from Pliocene modelling and data, *Nat. Geosci.*, *3*, 60–64, doi:10.1038/ngeo706.

Markwick, P. J. (1994), "Equability," continentality, and Tertiary "climate": The crocodilian perspective, *Geology*, *22*(7), 613–616, doi:10.1130/0091-7613(1994)022<0613:ECATCT>2.3.CO;2.

Markwick, P. J. (1998), Fossil crocodilians as indicators of Late Cretaceous and Cenozoic climates: Implications for using palaeontological data in reconstructing palaeoclimate, *Palaeogeogr. Palaeoclimatol. Palaeoecol.*, *137*, 205–271, doi:10.1016/S0031-0182(97)00108-9.

Marshall, J., D. Ferreira, M. J. Campin, and D. Enderton (2007), Mean climate and variability of the atmosphere and ocean on an aquaplanet, *J. Atmos. Sci.*, *64*(12), 4270–4286, doi:10.1175/2007JAS2226.1.

Matthews, E. (1984), Prescription of land-surface boundary conditions in GISS GCM II: A simple method based on fine-resolution data bases, *Tech. Memo 86096*, 20 pp., NASA Goddard Space Flight Cent. Inst. for Space Stud., New York.

McConnaughey, T. (1989a), 13 C and 18 O isotopic disequilibrium in biological carbonates: I. Patterns, *Geochim. Cosmochim. Acta*, *53*(1), 151–162, doi:10.1016/0016-7037(89)90282-2.

McConnaughey, T. (1989b), 13 C and 18 O isotopic disequilibrium in biological carbonates: II. In vitrosimulation of kinetic isotope effects, *Geochim. Cosmochim. Acta*, *53*(1), 163–171, doi:10.1016/0016-7037(89)90283-4.

Pagani, M., J. C. Zachos, K. H. Freeman, B. Tipple, and S. Bohaty (2005), Marked decline in atmospheric carbon dioxide concentrations during the Paleogene, *Science*, *309*, 600–603, doi:10.1126/science.1110063.

Pearson, P. N., and M. R. Palmer (2000), Atmospheric carbon dioxide concentrations over the past 60 million years, *Nature*, *406*, 695–699, doi:10.1038/35021000.

Pearson, P. N., N. J. Shackleton, and M. A. Hall (1993), Stable isotope paleoecology of middle Eocene planktonic foraminifera and multi-species isotope stratigraphy, DSDP Site 523, South Atlantic, *J. Foraminiferal Res.*, *23*(2), 123–140, doi:10.2113/gsjfr.23.2.123.

Pearson, P. N., P. W. Ditchfield, J. Singano, K. G. Harcourt-Brown, C. J. Nicholas, R. K. Olsson, N. J. Shackleton, and M. A. Hall (2001), Warm tropical sea surface temperatures in the Late Cretaceous and Eocene epochs, *Nature*, *413*, 481–487, doi:10.1038/35097000.

Pearson, P. N., B. E. van Dongen, C. J. Nicholas, R. D. Pancost, S. Schouten, J. M. Singano, and B. S. Wade (2007), Stable warm tropical climate through the Eocene Epoch, *Geology*, *35*(3), 211–214, doi:10.1130/G23175A.1.

Randall, D., R. Wood, and S. Bony (2007), Climate models and their evaluation, in *Climate Change 2007: The Physical Science Basis. Contribution of Working Group I to the Fourth Assessment Report of the Intergovernmental Panel on Climate Change*, edited by S. Solomon et al., chap. 8, Cambridge Univ. Press, Cambridge, U. K.

Roberts, C. D., A. N. LeGrande, and A. K. Tripati (2009), Climate sensitivity to Arctic seaway restriction during the early Paleogene, *Earth Planet. Sci. Lett.*, *286*(3–4), 576–585, doi:10.1016/j.epsl.2009.07.026.

Roche, D. M., Y. Donnadieu, E. Puceat, and D. Paillard (2006), Effect of changes in δ^{18}O content of the surface ocean on estimated sea surface temperatures in past warm climate, *Paleoceanography*, *21*, PA2023, doi:10.1029/2005PA001220.

Rogl, F. (1999), Mediterranean and Paratethys. Facts and hypotheses of an Oligocene to Miocene paleogeography (short overview), *Geol. Carpathica*, *50*(4), 339–349.

Royer, D. (2006), CO_2-forced climate thresholds during the Phanerozoic, *Geochim. Cosmochim. Acta*, *70*, 5665–5675, doi:10.1016/j.gca.2005.11.031.

Rull, V. (1999), Palaeoflorisitc and palaeovegetational changes across the Paleocene-Eocene boundary in northern South America, *Rev. Palaeobot. Palynol.*, *107*, 83–95, doi:10.1016/S0034-6667(99)00014-7.

Russell, G. L., J. R. Miller, and D. Rind (1995), A coupled atmosphere-ocean model for transient climate change studies, *Atmos. Ocean*, *33*(4), 683–730.

Russell, G. L., V. Gornitz, and J. Miller (2000), Regional sea level changes projected by the NASA/GISS atmosphere-ocean model, *Clim. Dyn.*, *16*, 789–797, doi:10.1007/s003820000090.

Scher, H. D., and E. E. Martin (2006), Timing and Climatic consequences of the opening of Drake Passage, *Science*, *312*(5772), 428–430, doi:10.1126/science.1120044.

Schmidt, G. A. (1999), Forward modeling of carbonate proxy data from planktonic foraminifera using oxygen isotope tracers in a global ocean model, *Paleoceanography*, *14*, 482–497, doi:10.1029/1999PA900025.

Schmidt, G. A., and S. Mulitza (2002), Global calibration of ecological models for planktic foraminifera from coretop carbonate oxygen-18, *Mar. Micropaleontol.*, *44*, 125–140, doi:10.1016/S0377-8398(01)00041-X.

Schmidt, G. A., G. R. Bigg, and E. J. Rohling (1999), Global Seawater Oxygen-18 Database, http://data.giss.nasa.gov/o18data/, Goddard Inst. for Space Stud., New York.

Schmidt, G., C. Bitz, U. Mikolajewicz, and L. Tremblay (2004), Ice-ocean boundary conditions for coupled models, *Ocean Modell.*, *7*(1–2), 59–74, doi:10.1016/S1463-5003(03)00030-1.

Schmidt, G. A., et al. (2006), Present-day atmospheric simulations using GISS ModelE: Comparison to in situ, satellite, and reanalysis data, *J. Clim.*, *19*(2), 153–192, doi:10.1175/JCLI3612.1.

Schmidt, G. A., A. N. LeGrande, and G. Hoffmann (2007), Water isotope expressions of intrinsic and forced variability in a coupled ocean-atmosphere model, *J. Geophys. Res.*, *112*, D10103, doi:10.1029/2006JD007781.

Schrag, D. P. (1999), Effects of diagenesis on the isotopic record of late Paleogene tropical sea surface temperatures, *Chem. Geol.*, *161*(1–3), 215–224, doi:10.1016/S0009-2541(99)00088-1.

Scotese, C. R., M. I. Ross, and A. Schettino (1998), Plate tectonic reconstruction and animation, *Eos Trans. AGU*, *79*, 334.

Sewall, J. O., L. C. Sloan, M. Huber, and S. Wing (2000), Climate sensitivity to changes in land surface characteristics, *Global Planet. Change*, *26*(4), 445–465, doi:10.1016/S0921-8181(00)00056-4.

Sexton, P. F., P. A. Wilson, and P. N. Pearson (2006), Microstructural and geochemical perspectives on planktic foraminiferal preservation: 'Glassy' versus 'Frosty', *Geochem. Geophys. Geosyst.*, *7*, Q12P19, doi:10.1029/2006GC001291.

Shackleton, N. J., and N. D. Opdyke (1977), Oxygen isotope and paleomagnetic evidence for early Northern Hemisphere glaciation, *Nature*, *270*, 216–219, doi:10.1038/270216a0.

Shukla, J., and Y. Mintz (1982), Influence of land-surface evapotranspiration on the Earth's climate, *Science*, *215*, 1498–1501, doi:10.1126/science.215.4539.1498.

Sloan, L. C., J. C. G. Walker, T. C. Moore, D. K. Rea, and J. C. Zachos (1992), Possible methane-induced polar warming in the early Eocene, *Nature*, *357*, 320–322, doi:10.1038/357320a0.

Sloan, L. C., M. Huber, and A. Ewing (1999), Polar Stratospheric Cloud Forcing in a Greenhouse World: Climate Modeling Sensitivity Study, in *Reconstructing Ocean History: A Window into the Future*, edited by F. Abrantes and A. Mix, pp. 273–293, Kluwer Acad., New York.

Sluijs, A., et al. (2006), Subtropical Arctic Ocean temperatures during the Palaeocene/Eocene thermal maximum, *Nature*, *441*, 610–613, doi:10.1038/nature04668.

Smith, R. S., C. Dubois, and J. Marotzke (2006), Global climate and ocean circulation on an aquaplanet ocean-atmosphere general circulation model, *J. Clim.*, *19*(18), 4719–4737, doi:10.1175/JCLI3874.1.

Solomon, S., D. Qin, M. Manning, Z. Chen, M. Marquis, K. Averyt, M. Tignor, and H. Miller (Eds.) (2007), *Climate Change 2007: The Physical Science Basis: Contribution of Working Group I to the Fourth Assessment Report on the Intergovernmental Panel on Climate Change*, Cambridge Univ. Press, Cambridge, U. K.

Spero, H. J., J. Bijma, D. W. Lea, and B. E. Bemis (1997), Effect of seawater carbonate concentration on foraminiferal carbon and oxygen isotopes, *Nature*, *390*, 497–500, doi:10.1038/37333.

Stone, P. (1978), Constraints on dynamical transports of energy on a spherical planet, *Dyn. Atmos. Oceans*, *2*, 123–139, doi:10.1016/0377-0265(78)90006-4.

Stroeve, J., M. M. Holland, W. Meier, T. Scambos, and M. Serreze (2007), Arctic sea ice decline: Faster than forecast, *Geophys. Res. Lett.*, *34*, L09501, doi:10.1029/2007GL029703.

Sud, Y. C., J. Shukla, and Y. Mintz (1988), Influence of land surface roughness on atmospheric circulation and precipitation: A sensitivity study with a general circulation model, *J. Appl. Meteorol.*, *27*(9), 1036–1054, doi:10.1175/1520-0450(1988)027<1036:IOLSRO>2.0.CO;2.

Tindall, J., R. Flecker, P. Valdes, D. N. Schmidt, P. Markwick, and J. Harris (2010), Modelling the oxygen isotope distribution of ancient seawater using a coupled ocean-atmosphere GCM: Implications for reconstructing early Eocene climate, *Earth Planet. Sci. Lett.*, *292*, 265–273, doi:10.1016/j.epsl.2009.12.049.

Toggweiler, J. R., and H. Bjornsson (2000), Drake Passage and palaeoclimate, *J. Quat. Sci.*, *15*(4), 319–328, doi:10.1002/1099-1417(200005)15:4<319::AID-JQS545>3.0.CO;2-C.

Tripati, A. K., and H. Elderfield (2004), Abrupt hydrographic changes in the equatorial Pacific and subtropical Atlantic from foraminiferal Mg/Ca indicate greenhouse origin for the thermal maximum at the Paleocene-Eocene Boundary, *Geochem. Geophys. Geosyst.*, *5*, Q02006, doi:10.1029/2003GC000631.

Tripati, A. K., and H. Elderfield (2005), Deep-sea temperature and circulation changes at the Paleocene-Eocene thermal maximum, *Science*, *308*, 1894–1898, doi:10.1126/science.1109202.

Tripati, A. K., J. Zachos, L. Marincovich, and K. Bice (2001), Late Paleocene Arctic coastal climate inferred from molluscan stable and radiogenic isotope ratios, *Palaeogeogr. Palaeoclimatol. Palaeoecol.*, *170*, 101–113, doi:10.1016/S0031-0182(01)00230-9.

Tripati, A. K., M. L. Delaney, J. C. Zachos, L. D. Anderson, D. C. Kelly, and H. Elderfield (2003), Tropical sea-surface temperature reconstruction for the early Paleogene using Mg/Ca ratios of planktonic foraminifera, *Paleoceanography*, *18*(4), 1101, doi:10.1029/2003PA000937.

Utescher, T., and V. Mosbrugger (2007), Eocene vegetation patterns reconstructed from plant diversity—A global perspective, *Palaeogeogr. Palaeoclimatol. Palaeoecol.*, *247*, 243–271, doi:10.1016/j.palaeo.2006.10.022.

Visbeck, M., J. Marshall, T. Haine, and M. Spall (1997), Specification of eddy transfer coefficients in coarse-resolution ocean circulation models, *J. Phys. Oceanogr.*, *27*(3), 381–402, doi:10.1175/1520-0485(1997)027<0381:SOETCI>2.0.CO;2.

Wefer, G., and W. H. Berger (1991), Isotope paleontology–Growth and composition of extant calcareous species, *Mar. Geol.*, *100*(1–4), 207–248, doi:10.1016/0025-3227(91)90234-U.

Weller, P., and R. Stein (2008), Paleogene biomarker records from the central Arctic Ocean (Integrated Ocean Drilling Program Expedition 302): Organic carbon sources, anoxia, and sea surface temperature, *Paleoceanography*, *23*, PA1S17, doi:10.1029/2007PA001472.

Wilf, P. (2000), Late Paleocene–Early Eocene climate changes in southwestern Wyoming: Paleobotanical analysis, *Geol. Soc. Am. Bull.*, *112*, 292–307, doi:10.1130/0016-7606(2000)112<292:LPECCI>2.0.CO;2.

Wilke, I., H. Meggers, and T. Bickert (2009), Depth habitats and seasonal distributions of recent planktic foraminifers in the Canary Islands region (29°N) based on oxygen isotopes, *Deep Sea Res., Part I*, *56*(1), 89–106, doi:10.1016/j.dsr.2008.08.001.

Wing, S. L. (1998a), Late Paleocene-early Eocene floral and climatic change in the Bighorn Basin, Wyoming, in *Late Paleocene-Early Eocene Biotic and Climatic Events*, edited by M.-P. Aubry, W. A. Berggren, and S. Lucas, pp. 371–391, Columbia Univ. Press, New York.

Wing, S. L. (1998b),Tertiary vegetation of North America as a context for mammalian evolution, in *Evolution of Tertiary Mammals of North America. Terrestrial Carnivores, Ungulates, and Ungulatelike Mammals*, vol. 1, edited by C. M. Janis, K. M. Scott, and L. L. Jacobs, pp. 37–60, Cambridge Univ. Press, Cambridge, U. K.

Wolfe, J. A. (1994), Tertiary climatic changes at middle latitudes of western North-America, *Palaeogeogr. Palaeoclimatol. Palaeoecol.*, *108*, 195–205, doi:10.1016/0031-0182(94)90233-X.

Wunsch, C. (2005), The total meridional heat flux and its oceanic and atmospheric partition, *J. Clim.*, *18*(21), 4374–4380, doi:10.1175/JCLI3539.1.

Zachos, J. C., L. D. Stott, and K. C. Lohmann (1994), Evolution of early Cenozoic marine temperatures, *Paleoceanography*, *9*(2), 353–387, doi:10.1029/93PA03266.

Zachos, J. C., M. Pagani, L. Sloan, E. Thomas, and K. Billups (2001), Trends, rhythms, and aberrations in global climate 65 Ma to present, *Science*, *292*, 686–693, doi:10.1126/science.1059412.

Zachos, J. C., M. W. Wara, S. Bohaty, M. L. Delaney, M. R. Petrizzo, A. Brill, T. J. Bralower, and I. Premoli-Silva (2003), A transient rise in tropical sea surface temperature during the Paleocene-Eocene Thermal Maximum, *Science*, *302*, 1551–1554, doi:10.1126/science.1090110.

Zachos, J. C., S. Schouten, S. Bohaty, T. Quattlebaum, A. Sluijs, H. Brinkhuis, S. J. Gibbs, and T. J. Bralower (2006), Extreme warming of mid-latitude coastal ocean during the Paleocene-Eocene Thermal Maximum: Inferences from TEX86 and isotope data, *Geology*, *34*(9), 737–740, doi:10.1130/G22522.1.

Zachos, J. C., G. Dickens, and R. E. Zeebe (2008), An early Cenozoic perspective on greenhouse warming and carbon-cycle dynamics, *Nature*, *451*, 279–283, doi:10.1038/nature06588.

Zeebe, R. E. (1999), An explanation of the effect of seawater carbonate concentration on foraminiferal oxygen isotopes, *Geochim. Cosmochim. Acta*, *63*(13–14), 2001–2007, doi:10.1016/S0016-7037(99)00091-5.

Zeebe, R. E. (2001), Seawater pH and isotopic paleotemperatures of Cretaceous oceans, *Palaeogeogr. Palaeoclimatol. Palaeoecol.*, *170*, 49–57, doi:10.1016/S0031-0182(01)00226-7.

Zeebe, R. E. (2007), An expression for the overall oxygen isotope fractionation between the sum of dissolved inorganic carbon and water, *Geochem. Geophys. Geosyst.*, *8*, Q09002, doi:10.1029/2007GC001663.

Zhang, J., and D. Rothrock (2000), Modeling Arctic sea ice with an efficient plastic solution, *J. Geophys. Res.*, *105*(C2), 3325–3338, doi:10.1029/1999JC900320.

Zhang, X., and J. E. Walsh (2006), Toward a seasonally ice-covered Arctic Ocean: Scenarios from the IPCC AR4 model simulations, *J. Clim.*, *19*, 1730–1747, doi:10.1175/JCLI3767.1.

Zhou, J., C. J. Poulsen, D. Pollard, and T. S. White (2008), Simulation of modern and middle Cretaceous marine δ^{18}O with an ocean-atmosphere general circulation model, *Paleoceanography*, *23*, PA3223, doi:10.1029/2008PA001596.

A. N. LeGrande, NASA Goddard Institute of Space Studies and Center for Climate Systems Research, Columbia University, 2880 Broadway, New York, NY 10025, USA.

C. D. Roberts, Met Office Hadley Centre, Fitzroy Road, Exeter, EX1 3PB, UK. (roberts.cd@gmail.com)

A. K. Tripati, Institute of the Environment, and Departments of Earth and Space Sciences and Atmospheric and Oceanic Sciences, University of California, 595 Charles Young Dr. E., Los Angeles, CA 90095-156, USA.